CHARACTERIZATION OF ENGINEERED TISSUE BY MULTIMODAL OPTICAL IMAGING AND BIAXIAL MECHANICAL TESTING

A Dissertation

by

YUQIANG BAI

Submitted to the Office of Graduate and Professional Studies of
Texas A&M University
in partial fulfillment of the requirements for the degree of

DOCTOR OF PHILOSOPHY

Chair of Committee,	Alvin T. Yeh
Committee Members,	Kayla J. Bayles
	Wonmuk Hwang
	Kenith Meissner
Head of Department,	Gerard L. Coté

May 2014

Major Subject: Biomedical Engineering

ABSTRACT

To better understand the relationships between mechanical stimuli and cellular responses, we developed a 3D tissue bioreactor coupling to both a biaxial mechanical testing platform and a stage for multimodal microscopy. Fibroblast seeded cruciform fibrin gels were investigated. A multimodal nonlinear optical microscopy-optical coherence microscopy (NLOM-OCM) system was developed to delineate relative spatial distributions of original fibrin, deposited collagen and fibroblasts non-invasively. Serial in-culture mechanical testing platform was also applied to track the evolution of bulk mechanical properties under sterile conditions. Wall stress depends on sample thickness and our multimodal imaging system measured evolving construct thickness as a function of mechanical stretch during biaxial tests. Through one month culture, cell and deposited collagen randomly distributed in non-stretched constructs. While under stretched condition, cell and deposited collagen fibers, which aligned with cell bodies, appeared preferentially parallel with principal stretch. Surprisingly both non-stretched and stretched constructs showed isotropic mechanical properties with increasing stiffness with culture time. In summary, our biaxial bioreactor system integrating both NLOM-OCM and mechanical testing provided complementary microstructural information and mechanical properties and thus may broaden fundamental understanding of soft tissue mechanics and mechanobiology.

DEDICATION

This dissertation is lovingly dedicated to parents, my wife and my daughter, for their support, sacrifice and love throughout my life.

ACKNOWLEDGEMENTS

I want to thank my advisor, Dr. Alvin T. Yeh, for his instruction and through my research in nonlinear tissue microscopy lab. His knowledge and remarkable insight helped me solved quite a lot of problems. He also spent a lot of time on improving my skills on writing papers. I also want to give thanks to my committees, Kayla J. Bayless, Kenith Meissner, Wonmuk Hwang, and previous members of Roland R. Kaunas, Jay D. Humphrey, for their invaluable advice on my research. Thanks were also gave to my friends in Texas A&M University: Po-feng Lee, Holly Gibbs, and Qiaofeng Wu for their great advice on the project. At last, thank my parents, my wife for their unfailing love.

TABLE OF CONTENTS

Page

LIST OF FIGURES

Page

CHAPTER I

INTRODUCTION

It is well-accepted that the rate of synthesis, degradation and alignment of collagen were influenced by mechanical stimuli, but the rules to describe these processes are still under wanted. Various fields dealing with connective tissues such as morphogenesis [1], tissue engineering [2], wound healing [3], and soft tissue growth and remodeling [4, 5] would be benefited by such rules. Experiments with simple conditions will simplify results analysis, thus further our insights in these processes. We propose that serial observations of engineered tissues with simplified boundary conditions will increase the insights about how mechanical stimuli affect the properties of deposited collagen in soft tissues.

1.1 Motivation

There are plenty of information known about collagen: the amino acid sequence of collagen's triple-helical structure; [6-7] genes on transcriptional features of collagen; [8-11] collagen's translational pathways. [12-13] It is already know that collagen synthesis are controlled by intracellular accumulation; [14-15] that molecules can self-assemble into fibrils, which can form collagen fibers with diameters of microns; [16-18] that stimulation can affect the process of collagen production and degradation; [19-21] the kinds of proteases that can degrade collagen. [22-25] However, detailed descriptions of rates of deposition and degradation remain required. Growth and remodeling about aneurysm was studied [26], but information within stress (or stretch) controlled collagen deposition still under wanted .

Thus, needs for theories motivate simple experiments that can synthesize obtained data and enlarge the knowledge base for native tissues and eingineered tissues.

One of most straightforward approaches to understanding relationships between tissue (i.e., 3D) mechanics and cellular responses is simply to study responses of cell-seeded tissue constructs cultured under different mechanical environments.[27-32] Typically Prajapatic et al[33] reported a method to vary the loading conditions over the course of culture. Tissues embedded with cells were subjected to varying loads controlled by computers. However most of these studies were restricted to uniaxial loadings and several days however. Uniaxial loading and related measures provided useful information about tissues' mechanical properties. Yet, mechanical anisotropy complicated uniaxial data to estimate parameter in constitutive equations. In order to test hypotheses of tissue growth&remodeling, it is necessary to design experiments that provide simple boundary conditions and simplify the analysis of results. And, responses of tissue to mechanical environment (i.e. growth and remodeling) usually take weeks or months instead of hours or days. Knezevic et al [34] described a system within which cell-matrix constructs were subjected to biaxial loads. Square fibroblast-populated gel with porous were loaded by hanging weights. The weights could be changed anytime during culture. This was an important advance by applying biaxial loading on engineered tissues.

To characterize underlying tissue microstructure under various mechanical conditions, optical methods have shown great promise for nondestructively characterizing parameters of 3D matrices including microstructural organization,

porosity/pore size, and local matrix remodeling, and cell responses to these parameters including migration and morphology.[35-44] Small angle light scattering (SALS) techniques were coupled with mechanical testing to correlate stress-strain relations and fiber microstructure,[45] optical clearing by hyperosmotic agent altered tissues' properties,[46] thus it was difficult to correlate macroscopic properties with microstructures. Confocal microscopy utilizing image stacks has provided three-dimensional renderings of tissue architecture with micrometer resolution. [35, 47] Voytik-Harbin et al [29] reconstructed the 3-D alignment of collagen fibers by confocal microscopy. Yet, the need for exogenous labels or the lack of chemical specificity can complicate serial measures of tissue microstructure and the interpretation of microscopic events, such as deposition of new collagen matrix within an existing fibrin network.[47]

In summary, experimental problems including "longitudinal" biaxial mechanical characterization and obtaining comprehensive microstructures information within most common approaches impeded our way to understanding the relationships between mechanical conditionings and cellular responses which in turn elicit matrix deposition and bulk mechanical evolving. The studies performed here used an biaxial bioreactors that were designed and constructed to culture cruciform-shaped constructs under well-defined mechanical stretch, to perform longitudinal non-destructive force–extension tests on these constructs, and to characterize evolving microstructural composition and organization noninvasively, and thus, may enable greater fundamental understanding of relationships between engineered soft tissue mechanics and mechanobiology.

1.2 NLOM-OCM imaging system

Different optical microscopy techniques, like optical coherence microscopy (OCM), [38-39] and confocal microscopy, [35-37] have been widely used in biomedical research with the advantages of non-invasive, high speed, and high resolution imaging of structure and biology of the sample. Combination of different imaging modalities provided complementary information of the sample. In this study, we developed a integrated NLOM-OCM imaging system based on sub-10-fs Titanium:Sapphire laser to image different components. OCM has an advantage in imaging depth by combining interferometry with confocal pinhole. Multi-photon excited fluorescence, [40] second harmonic generation (SHG), [41, 42] and stimulated Raman signal [43, 44] have been used to image thin sections within thick, living biological tissues nondestructively. NLOM provides detailed information about the extracellular matrix, such as collagens fibers and mature elastin, without exogenous labels.[48, 49] Tan *et al* [50] demonstrated the integration of NLOM with OCM in 3D cultures. Herein, we exploited the ability of integrated NLOM-OCM utilizing sub-10-fs pulses to characterize interactions between cell and extracellular matrix (ECM) in engineered constructs , including fibrin matrix seeded with neonatal human dermal fibroblasts in which new fibrillar collagen is synthesized during culture.

1.3 Bioreactor with mechanical testing platform

To enable serial in-culture mechanical testing and imaging without compromising sterility, our previous bioreactor [48] was refined with several modifications. First, an immersible 50 g force transducer (Honeywell) was integrated in line on each axis by a

polycarbonate adapter. All parts were assembled, immersed within 70% ethanol, and air dried before use. In this way, serial mechanical tests were performed directly within the sealed bioreactor during culture, avoiding possible damage or contamination by transferring to a separate mechanical testing device. There are two different covers for each chamber. One is used during culture and mechanical testing, and the second is used for the intravital imaging which keeps engineered tissue sterile.

1.4 Characterization of engineered tissues

Among various types of scaffold for tissue engineering, [52-58] fibrin has been identified as a new biopolymer scaffold with a number of advantages. One advantage is that fibrin gel stimulates deposition of collagen.[59-63]To explore how cells response to various mechanical stimuli, we chose fibrin as primary scaffold to characterize collagen deposition and organization. With addition of thrombin, fibrinogens form fribrin fibrils, therefore it forms a tissue similar to collagen gel, and could be subjected to various different mechanical stimuli. Fibroblast seeded fibrin gels were investigated through 31 days. NLOM-OCM delineated relative spatial distributions of collagen, fibrin, and fibroblasts non-invasively using endogenous contrast. Additionally, with the appropriate objective, the integrated imaging system was utilized to complete mechanical testing by measuring construct thickness as a function of stretch to derive Cauchy (true) stress.

1.5 Outline

In the following, the integrated NLOM – OCM imaging system is described in Chapter II. The bioreactor enabling serial mechanical testing and optical imaging was described in Chapter III. Chapter IV describes how the combined NLOM-OCM

measured microstructural and evolving mechanical properties response as a function of stimuli. Finally in Chapter V the conclusions of this study and future work are discussed.

CHAPTER II

INTEGRATION OF NONLINEAR OPTICAL MICROSCOPY - OPTICAL COHERENCE MICROSCOPY*

Understanding interactions between cells and extracellular matrix has progressed with the development and use of 3D tissue models. A consequence of performing these studies in 3D matrices rather than in 2D cell culture is the dramatic differences in cell adhesions with the scaffold/substrate in structure, localization, and function. Thus, studies characterizing cell-matrix interactions may be more biologically relevant when utilizing 3D tissue models.[64] The popular matrices include collagen type I gels, [65-69] cell-derived matrix,[70-71] fibrin gels,[72] and basement membrane extract.[73] Fibrin gels in particular have exhibited promising properties with better bulk properties and stimulation of more collagen and elastic fiber synthesis and deposition when compared to collagen gels.[74] Generally, these studies have focused on a single specific 3D model, and, when possible, a reconstituted matrix with the simplest necessary component thereby enabling dissection of matrix protein functions. Also, current microscopy technology has demonstrated the capability to characterize cell-matrix interactions in these 3D environments over a time course. However, tissues in living organisms can vary substantially in matrix composition and present resident cells with multiple matrix

---

*Part of the data reported in this chapter is reprinted with permission from "Dynamic multicomponent engineered tissue reorganization and matrix deposition measured with an integrated nonlinear optical microscopy–optical coherence microscopy system", Bai Y, et al. J. Biomed. Op, 19(3):036014. Copyright [2014] SPIE.

proteins which may have synergistic and/or competing/antagonistic functions. Thus, multicomponent models may be used as a viable approach to characterize cell interactions in tissue environments more similar to in vivo. Yet, additional matrix components challenge current microscopy techniques in segmentation and delineating cell responses non-invasively and non-destructively through an experimental protocol. Here, we illustrated the application of integrated nonlinear optical microscopy – optical coherence microscopy in the characterization and delineation of 3D tissue remodeling and matrix deposition in a multicomponent system composed of fibrin and collagen seeded with fibroblasts.

2.1 Integration of NLOM-OCM imaging system

In this study, a combined NLOM-OCM system based on sub-10-fs Titanium:Sapphire laser was developed to simultaneously image components of the sample. A schematic setup is shown in Figure 2.1. Briefly a titanium:sapphire oscillator generating sub-10-femtosecond pulses with central wavelength at 800 nm and 130 nm full-width-at-half-maximum (Femtosource, Femtolasers) was used as a common source for both NLOM and OCM. The integrated NLOM-OCM system utilized a Michelson interferometer configuration where one arm was directed to the tissue construct for both NLOM and the sample arm of OCM while the other was used as the reference arm for OCM. NLOM signals generated from the sample were directed to a two-channel detector for image rendering at two different wavelengths for second harmonic generation (SHG) in collagen and two-photon excited fluorescence (TPF) in cells. Backscattered laser light from the sample was combined with the return beam of the reference arm and directed to

a custom spectrometer for Fourier-domain OCM. Integration of NLOM and OCM enabled microscopic tissue characterization using simultaneously acquired imaging signals that are both constituent specific (nonlinear optical signals) and non-specific (backscattered laser light). For thickness measurements, a low numerical aperture objective provided a long depth of focus to render cross-sectional images by optical coherence tomography (OCT).

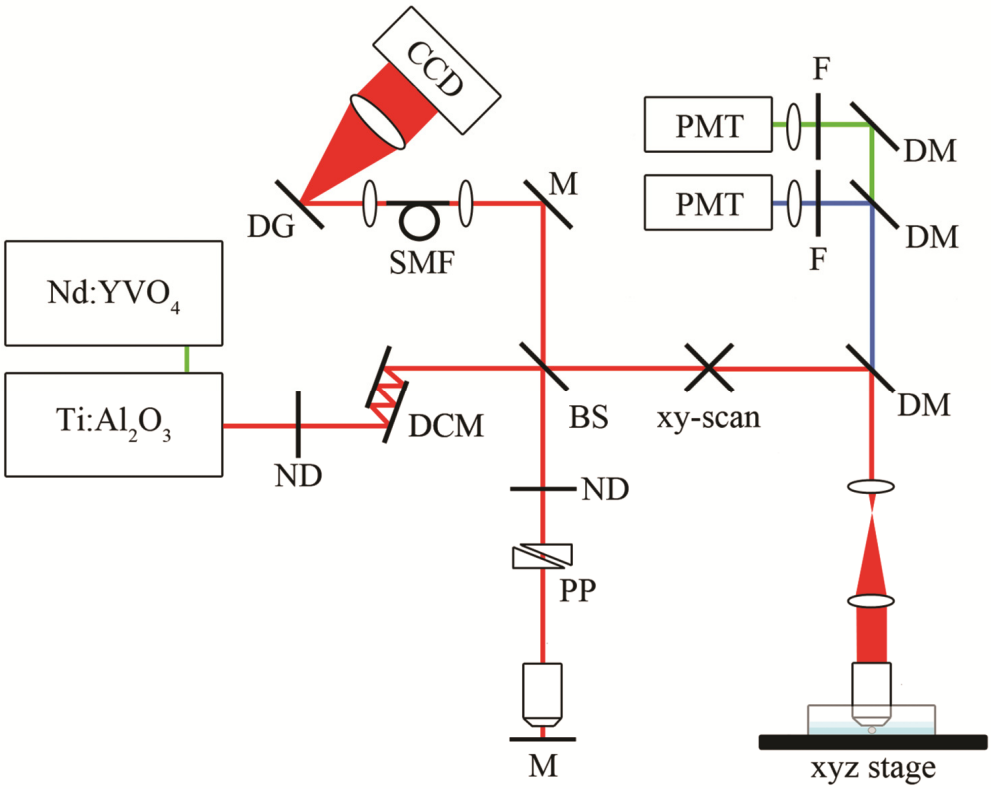

Fig 2. 1 Schematic diagram of NLOM-OCM set up: BS, beam splitter; CCD, charge-coupled detector; DCM, dispersion chirp mirror; DG, diffraction grating; DM, dichroic mirror; F, filter; L, lens; M, mirror; PP, pair prism; PMT, photomultiplier tube; SMF, single-mode fiber.

2.2 Application of NLOM-OCM

Without the use of exogenous agents, both OCM and NLOM rely on spatial inhomogeneities in tissues to provide image contrast. OCM maps the local linear tissue optical scattering properties and NLOM relies on differences in the local nonlinear optical properties of tissue. These complementary contrast mechanisms enabled label-free imaging of fibrin, in which nonlinear optical signals have not been observed, and collagen using endogenous signals. Thus, we used NLOM-OCM to characterize and delineate remodeling of intertwined collagen and fibrin fibers by seeded fibroblasts. In addition in 3D fibrin matrices, we used NLOM-OCM to image and characterize deposited collagen anisotropy by embedded fibroblasts over time, cultured under different boundary conditions.

2.2.1 Application in Fibrin gel

An advantage of integrating OCM with NLOM is the capability of rendering optically sectioned images without relying solely on nonlinear optical signals. This capability is useful in tissue systems such as reconstituted fibrin matrices in which nonlinear optical signals TPF and SHG are not readily observable. OCM images of unlabeled fibrin gels are shown in Fig 2.2 at concentrations of 5 mg/ml (Fig 2.2A), 7.5 mg/ml (Fig 2.2B), 10 mg/ml (Fig 2.2C), and 15 mg/ml (Fig 2.2D). The OCM images show that fibrin porosity increases with decreasing concentration. Fibrin fibers appeared straight, rod-like structures, particularly at low concentrations (<10 mg/ml). At high fibrin concentrations, straight, rod-like structures were not as evident, possibly due to aggregation, giving way to a more bulbous morphology, cf., Fig 2.2D.

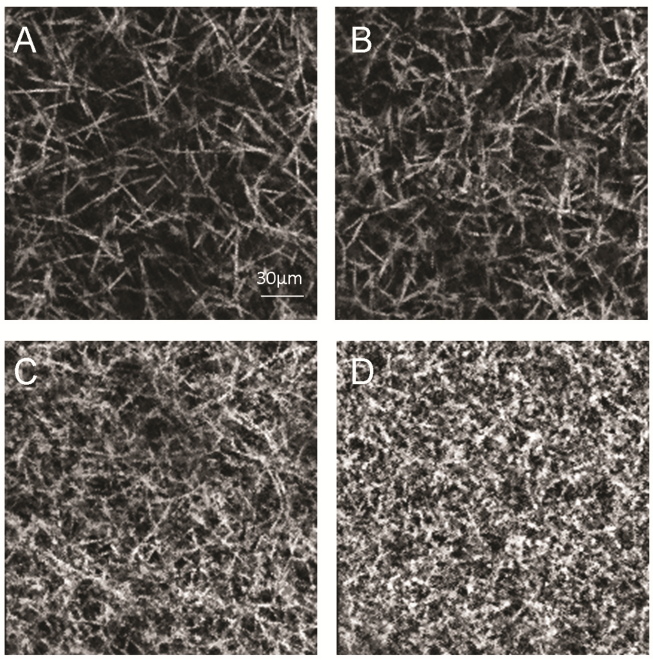

Fig 2. 2 Representative images of fibrin gel. (A)-(D) 5mg/ml, 7.5mg/ml, 10mg/ml, 15mg/ml. The fibers are straight rod-like structures at all fibrin concentrations. Gel porosity decrease with increasing fibrin concentration. Scale bar: 30µm.

2.2.2 Application in fibrin and collagen gel mixtures

Fibrin fiber imaging with OCM is non-specific. Thus, if collagen was mixed into the fibrin gel, imaging signals from OCM could not be easily processed to differentiate between the two matrix proteins. However, SHG in collagen is readily observable, constituent specific, and may be used to segment it from fibrin. Serial images acquired by integrated NLOM-OCM, in which NLOM and OCM images are simultaneously acquired, are shown in Fig 2.3 of NIH 3T3 cell seeded fibrin-collagen mixture matrix. Total protein concentration was 5 mg/ml with 9:1 ratio of fibrin:collagen, i.e., 4.5:0.5 mg/ml. NLOM-OCM images from two representative regions are shown at three time

points (1, 12, 24 hours) from a time series containing two 3T3 cells (upper images) and from an acellular region (lower images). Specifically, TPF from the two regions are shown for the three time points in Fig 2.3A. Cellular autofluorescence indicated two cells within the field-of-view that extended processes over 24 hours (Fig 2.3A, upper images). No TPF was detected from the acellular region (Fig 2.3A, lower images). Images rendered using SHG are shown in Fig 2.3B which identified a subset of collagen fibers within the composite matrix. In cellular (upper images) and acellular regions (lower images), an increase in collagen density was observed, though the increase in collagen density was more pronounced in the cellular region. Non-specific OCM image simultaneously acquired with NLOM (TPF and SHG) is shown in Fig 2.3C. OCM images rendered from backscattered laser light revealed a predominantly fibrous morphology. NLOM-OCM images were overlaid and are shown in Fig 2.3D with cellular TPF, collagen SHG, and OCM false colored blue, red, and green, respectively. In this simple three component tissue construct, OCM structures not overlapping with NLOM (TPF and SHG) were assumed to be fibrin and, thus, green in Fig 2.3D. The overlaid images in Fig 2.3D revealed dynamic relative spatial distributions of 3T3 cells, collagen, and fibrin that occurred in remodeling of the tissue.

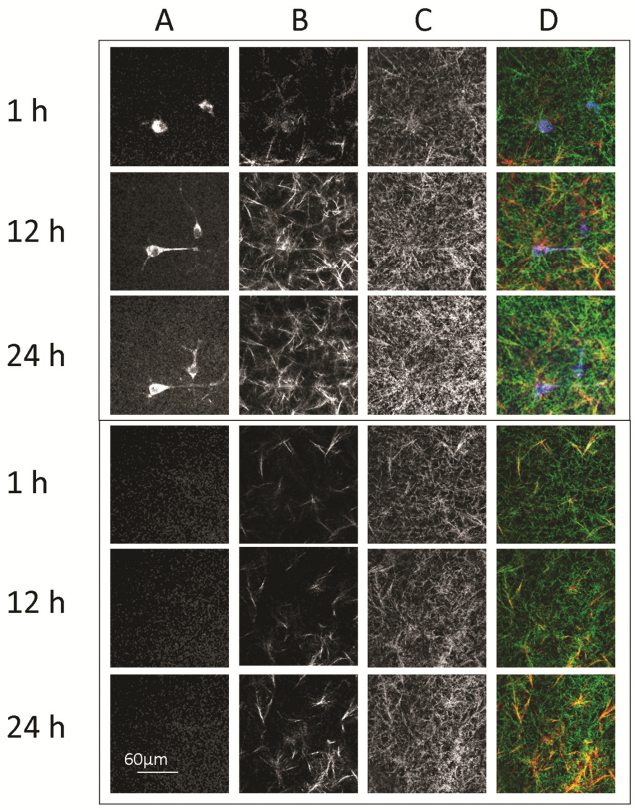

Fig 2. 3 Series of NLOM-OCM images of fibroblasts seeded in collagen-fibrin gel. (A) Cellular autofluorescence by TPF. (B) SHG in collagen. (C) Nonspecific OCM image. (D) False color overlay showing fibrin (green), collagen (red), and cell (blue). Scale bar: 60µm.

2.2.3 Application in evolving engineered tissues

With the ability to segment collagen (and cells) from fibrin fibers in composite matrices, NLOM-OCM was used to image collagen deposition and matrix remodeling in fibroblast seeded fibrin gels. For this study, neonatal human dermal fibroblasts (NHDF) were used instead of NIH 3T3 cells because of their comparatively robust translation of collagen protein. Also, NHDF were transfected with GFP-vinculin plasmid to aid in imaging of cell morphology, especially at depth. NHDF seeded cruciform-shaped fibrin gels (5 mg/ml) were cultured under three different mechanical boundary conditions,

anchored at 1.0:1.0, strip biaxial at 1.0:1.1, and equibiaxial at 1.1:1.1 stretch ratios (see Fig 2.4).

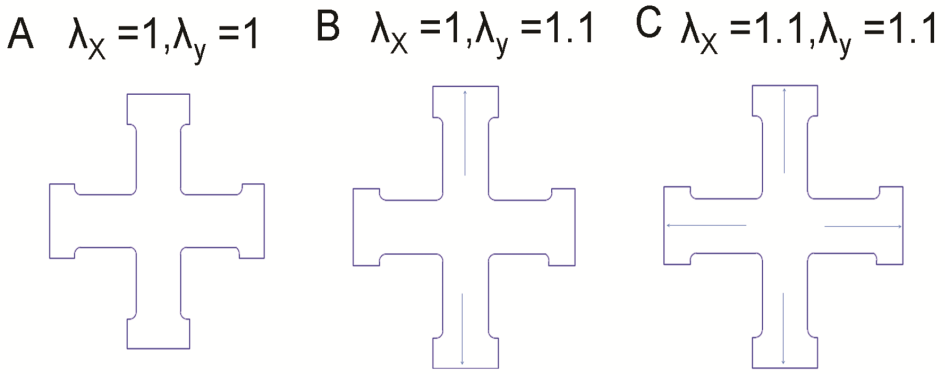

Fig 2. 4 Protocols of stretching: (A) 1.0:1. 0(B) 1.0:1.1. (C) 1.1:1.1. Data were acquired from the sample's central region.

Images of fibrin gels were acquired during 17 days of culture from the gel's center and analyzed to quantify fibrin and collagen fiber orientation distributions. Representative NLOM-OCM images of anchored (1.0:1.0) fibrin gels are shown in Fig 2.5 from Days 1, 3, 10, and 17. TPF images in Fig 2.5A show NHDF initially round (Day 1) that by Day 3 have elongated and extended processes, and population of cells gradually increaseed coinciding with an increase in cell density. Images rendered from SHG and shown in Fig 2.5B suggested NHDF deposition of collagen that accumulated over time. Overlay images of TPF and SHG are shown in Fig 2.5C that are false colored green and red, respectively. The overlay images showed the relative distribution of NHDF and deposited collagen, much of which appeared to be aligned with cell bodies. OCM images are shown in Fig 2.5D. Fibrin fiber and NHDF morphology were distinct

on Day 1, but at later times, the fibrin gel has compacted such that OCM image contrast was dominated by its density. We note that NLOM-OCM images from NHDF seeded fibrin gels cultured under equibiaxial stretch exhibited qualitatively similar results and, thus, not shown, but were analyzed for matrix.

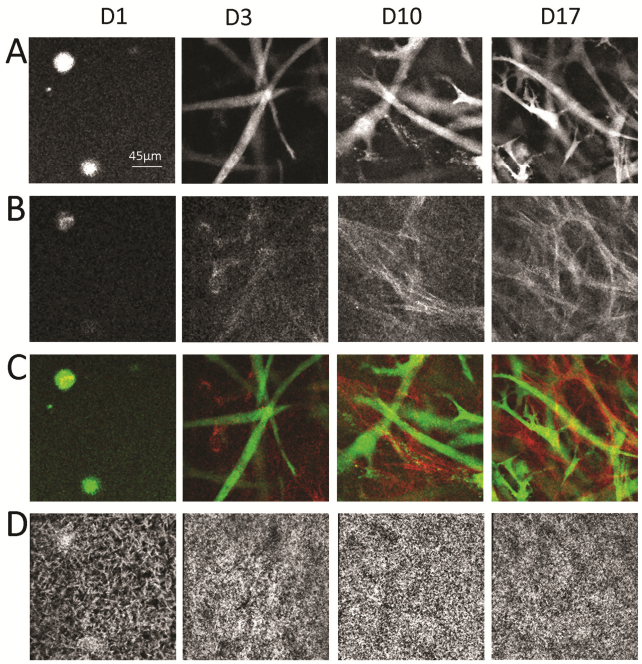

Fig 2. 5 Representative NLOM-OCM images of fibroblasts seeded in fibrin gel with 1:1 stretch ratio on day 1, 3, 10, 17. (A) Cellular fluorescence by TPF. (B) SHG in collagen. (C) False color overlay showing collagen (red), and cell (green). (D)Nonspecific OCM image. Scale bar: 45µm.

An important parameter in engineering tissues is the (an) isotropy or predominant angle and distribution of deposited matrix. Results from anchored fibrin gels suggested that NHDF deposit collagen parallel with its cell body, thus, by controlling cell alignment, it may be possible to control alignment of deposited matrix. To test this hypothesis, NHDF seeded fibrin gels were cultured under strip biaxial stretch (1.0:1.1 stretch ratio). Representative NLOM-OCM images from the central region are shown in

Fig 2.6 from 17 days in culture; the principal stretch axis is oriented vertically in the images. TPF images are shown in Fig 2.6A and, consistent with anchored fibrin gels, NHDF morphology was initially rounded on Day 1 and had elongated and extended processes by Day 3. Of note is that elongated cells appeared to preferentially align with principal stretch. SHG images are shown in Fig 2.6B and indicated an accumulation of collagen with culture time. Collagen within the SHG images appeared to preferentially align with cells in the direction of principal stretch. Overlay images of TPF and SHG images are shown in Fig 2.6C false colored green and red, respectively.

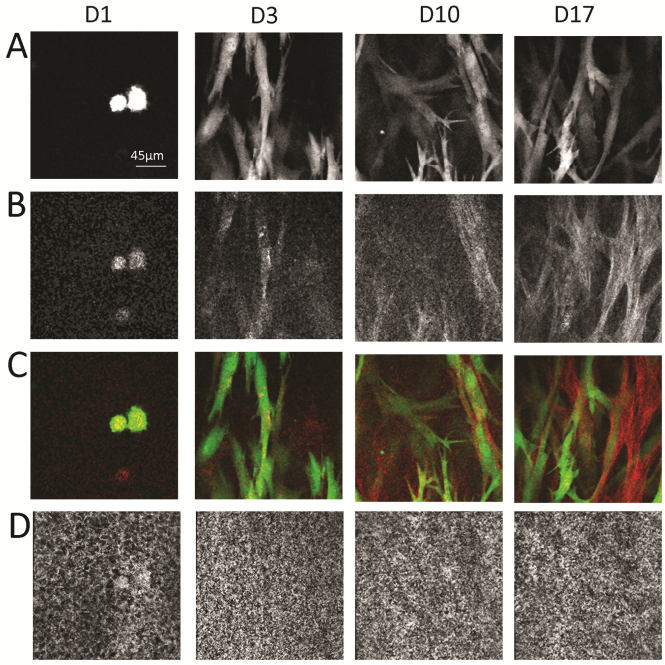

Fig 2. 6 Representative NLOM-OCM images of fibroblasts seeded in fibrin gel with 1:1.1 stretch ratio on day 1, 3, 10, 17. (A) Cellular fluorescence by TPF. (B) SHG in collagen. (C) False color overlay showing collagen (red), and cell (green). (D)Nonspecific OCM image. Scale bar: 45µm.

OCM images are shown in Fig 2.6D in which, similar to anchored fibrin gels, contrast was dominated by the dense fibrin matrix. (Over the course of 24 hours, NHDF

seeded fibrin gels thinned from ~1 mm to ~0.1 mm, regardless of culture boundary conditions.) NLOM-OCM images from three stacks acquired from the central region of NHDF seeded fibrin gels were analyzed to quantify matrix fiber orientation over 17 days of culture, and the results are shown in Fig 2.6. Matrix fiber angle distributions are shown for anchored gels in Fig 2.6A. For Day 1, OCM images were used to calculate fibrin fiber orientation distributions. Fibrin fibers exhibited an isotropic orientation distribution, also reflected in its calculated alignment index, AI = 1.0948. For later time points on Days 3, 10, and 17, SHG images were analyzed to calculate deposited collagen fiber orientation distributions; analysis of OCM images for these time points exhibited isotropic fibrin fiber angle distributions (data not shown). In anchored gels, no preferential alignment was exhibited. Consistent with these results for anchored gels, analysis of fibrin and collagen fiber angles in equibiaxially stretched gels also exhibited isotropic distributions. These isotropic distributions are shown in Fig 2.7B, with AI = 1.1068 for fibrin fibers on Day 1 and 1.1743, 1.1557, and 1.2381 for deposited collagen fibers on Days 3, 10, and 17, respectively.

Analyses of matrix fiber angle distributions of strip biaxially stretch gels are shown in Fig 2.7C. Despite a principal stretch of 10%, fibrin fiber angles exhibited isotropic distribution with an AI = 1.1227. Yet, this principal stretch was enough to induce NHDF alignment and consequent anisotropic collagen deposition as early as Day 3 as evidenced by collagen fiber angle distribution with AI = 1.2955 (predominant angle at 0° coincident with principal stretch axis).

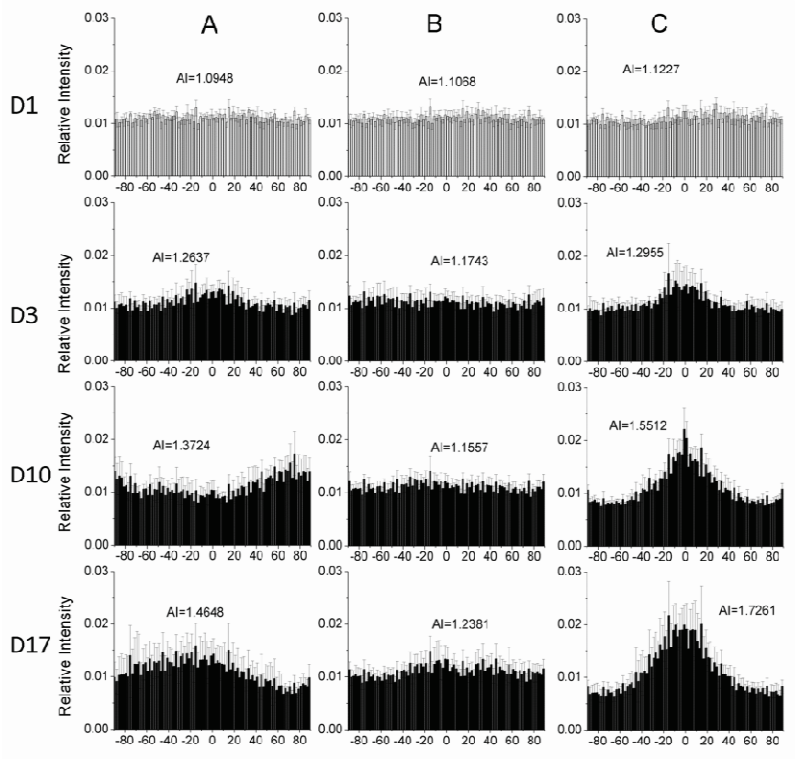

Fig 2. 7 Analyses of initial fibrin fiber on day 1 and deposited collagen fiber distribution of central region on day 3, 10, 17. (A). 1:1 stretch ratio. (B). 1.1:1.1 stretch ratio. (C) 1.0:1.1 stretch ratio.

The collagen fiber angle distribution sharpened with culture time along the principal stretch axis with increasing AI, 1.5512 and 1.7261 on Days 10 and 17, respectively. It should be noted that fibrin fiber angles exhibited isotropic distributions for each of the days (data not shown).

2.3 Discussion

An integrated NLOM-OCM system based on sub-10-fs pulses was developed to characterize dynamic matrix remodeling and collagen deposition within cell seeded (mixed collagen-fibrin and fibrin) gels. An advantage of the near-infrared wavelength source used for NLOM-OCM was its ability to image deeper into turbid, biological

tissues, especially when compared with visible sources used for laser scanning confocal microscopy. Use of the common ultrashort pulse laser source helped facilitate simultaneous acquisition of NLOM and OCM images. Inherently short coherence length and high peak power of pulses helped ensure localization of imaging signals to microscopy focus. However, depth of imaging into turbid biological tissue differed for NLOM and OCM primarily because of different signal wavelengths—higher scattering of NLOM signals (SHG and TPF in visible wavelength region) than near-infrared OCM signal. Nevertheless, previous implementations of integrated NLOM-OCM have recognized the advantages of combining techniques with complementary contrast mechanisms.[75-76] Here, these complementary techniques were used to non-invasively image multicomponent tissue constituents, a subset of which had observable endogenous NLOM (TPF and SHG) signals. In these tissue systems, OCM provided context to the images of constituents with nonlinear contrast, i.e., global view of tissue microenvironment morphology, albeit without inherent chemical specificity.

CHAPTER III

BIOREACTER WITH BIAXIAL MECHANICAL TESTING

Many soft connective tissues, ranging from skin to arteries, experience multiaxial mechanical loading in vivo and exhibit diverse responses to these environments, including growth and remodeling, injury, and repair. These responses are mediated by resident and recruited cells through proliferation, degradation, migration, traction, matrix reorganization, deposition, or apoptosis, which may alter the cellular mechanical environment and, in turn, elicit further cellular responses. This interaction between cells and matrix has been proposed to achieve, maintain, or restore a mechanobiological equilibrium or homeostasis (e.g., tensional [77]). Indeed, mechanical conditioning of tissue engineered constructs has been used to elicit seeded cell responses to generate tissues having more physiological properties than statically loaded constructs alone, with the ultimate goal that these constructs emulate and integrate within native tissues.[78] Yet, understanding relationships between mechanical environments and cellular responses (i.e., the mechanobiology), and using these relationships to guide tissue morphogenesis in culture remain challenging.

One approach to understanding relationships between tissue (i.e., 3D) mechanics and cellular responses is simply to study responses of cell-seeded tissue constructs cultured under different mechanical environments. Different platforms have been developed that can characterize tissue mechanical stimuli uniaxially or biaxially and the underlying microstructural organization. [28, 79]

Here, we describe a biaxial tissue culture platform designed to culture cruciform-shaped constructs under defined mechanical stretch, to perform longitudinal non-destructive mechanical tests on these constructs, and to characterize the microstructural composition and organization noninvasively using a multimodal imaging system.

3.1 Bioreactor

3.1.1 Bioreactor

To enable serial in-culture mechanical testing and imaging without compromising sterility, a custom bioreactor was built to impart stretches, to enable intravital imaging and mechanical testing. The inner of bioreactor has cruciform shape and is made of 2 inch thick polycarbonate with a removable top. One loading carriage per axis house a force transducer mounted inside the chamber.

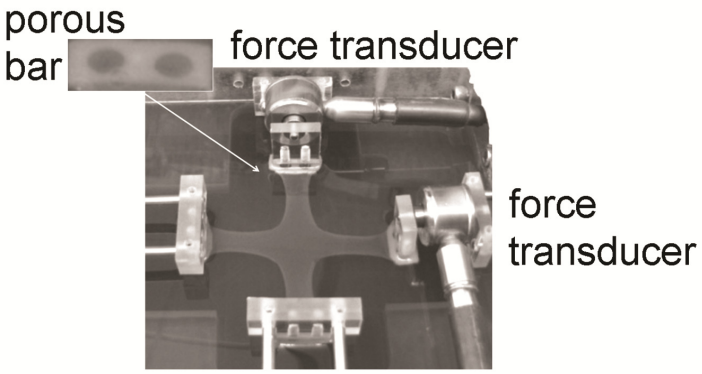

Fig 3. 1 Photograph of gel(measuring end to end 7.3cm) coupled to load bars of biaxial bioreactor. Notice the single force transducer fitted on each axis. The four load arms were attached to the construct via two posts that projected from the bottom of polycarbonate end pieces; these posts inserted in two holes within the porous polyethylene bars positioned at the ends of the cruciform construct. Upper left corner: porous bar coupling end of gel arm.

Customized porous bars (Small Parts, Miramar, FL), each punctured with two holes by which gel was anchored in the bioreactor (see details in Fig 3.1), were

positioned within the cruciform mold before adding solutions. By this way cruciform-shaped gels could be stretched with various ratio, such as: 1.01:1.01; 1.01:1.1; or 1.1:1.1 stretch (as shown in Fig 2.4). The bioreactor was kept in an incubator except when tested or imaged.

All parts were assembled, immersed in 70% ethanol, and air dried before use. In this way serial mechanical tests were performed directly within the bioreactor during culture, avoiding possible damage caused by gripping or 'contamination' by transferring from culture device to mechanical testing device. Moreover, a polycarbonate lid with a center hole sealed with optical quality glass was used during tissue culture and for viewing tissue embedded microbeads during mechanical testing. Another polycarbonate lid fitted with a window assembly was used for in-culture microscopic imaging (Fig 3.2). The window assembly consisted of a plastic bushing, glass tube with O-ring and coverslip bottom, and glass adapter as seen in Fig 3.2A. The position of the glass tube with coverslip bottom was adjusted to contact the tissue construct during microscopic imaging. The completed assembly is shown in Fig 3.2B. Compression of the glass tube o-ring formed a seal with the glass adapter, and the bushing was glued into the lid to complete the seal. The lids were all sealed with silicone rubber gasket and secured on top of the culture chamber by screws and switched under aseptic conditions in a class II biosafety cabinet. Finally sleeve bearings where the stainless steel rods traverse the wall of bioreactors were sealed with silicone rubber to protect the 'inner sterility'. With above improvements, 'sterility' was maintained for at lease one month culture with frequent optical microscopic imaging and mechanical testing.

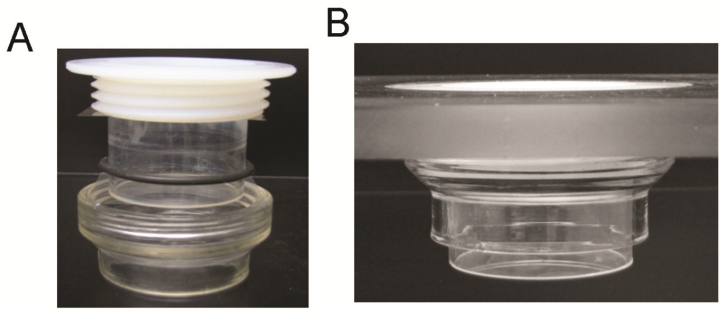

Fig 3. 2 Window assembly for intravital microscopic imaging. (A) Top to bottom: bushing, glass tube with an O-ring and coverslip bottom, and glass adapter. Tube sits in the adapter by o-ring, then bushing is screwed into the glass adapter to seal the tube by compressing o-ring. (B) Assembly sits in polycarbonate lid and is sealed by glue.

3.1.2 Mechanical testing platform

A home-built computer-controlled biaxial loading platform was used to mechanically test the tissue constructs within the bioreactor.[80] During testing, the bioreactor was placed on the loading platform and each of the four load bars was attached to a high travel resolution (0.01 μm) stepper motor (Parker, OH) located at each corner of the square platform. Stepper motors were controlled from positions of microspheres within the gel. A CCD camera mounted above the bioreactor and positioned over the glass sealed central hole of the bioreactor lid was used to monitor positions of at least four embedded microbeads. Images were captured via a video frame grabber board, which digitized the image to a 256×256 pixel matrix. The program computed the deformation gradient. Force and displacement data were recorded along with the process.

3.1.3 Thickness Measurement

The intrinsic optical sectioning capability of sub-10-fs pulse ultrashort coherence length was also used to render cross-sectional images for measurement of tissue thickness. OCM en face image acquisition was switched to cross-sectional (B-scan) optical coherence tomography (OCT) with use of a low numerical aperture objective (1× Achroplan, 0.025 NA). Cross-sectional OCT images were rendered from a sequence of axial reflectance depth profiles (A-line) by laterally scanning the laser focus across the tissue. Each A-line was acquired in a single shot in the Fourier domain. Fourier-domain OCT [81] can generate A-lines without scanning a reference mirror, thus eliminating a source of noise and greatly increasing imaging speed. In FD-OCT, all scatterers in an A-line are simultaneously measured then contribute to the interference signal. This interference signal is caculated in frequency domain via a spectrometer based on a diffraction grating and CCD camera. Each A-line contributed to a B-scan image by Fourier transform of the spectrum of the interferogram. Image data were averaged three times to increase signal-to-noise ratio (SNR).

After mechanical testing, construct thickness was measured at different stretch ratios from cross-sectional images acquired by OCT. Specifically, the construct was stretched within testing rig to pre-set biaxial values, locked in the deformed configuration by set screws on the loading arms, transferred to the microscopy stage for OCT imaging, replaced on the mechanical testing rig, and returned to the original configuration before stretching to the next position for OCT measurement.

3.2 Results

3.2.1 Comprehensive testing protocols

As shown in Fig 3.3, construct was preconditioned through 3 cycles of 15% equibiaxial stretch followed by three stretch protocols (Fig 3.3A), namely, (1) Y-direction strip biaxial, (2) equibiaxial, and (3) X-direction strip biaxial stretch. The load-stretch curves of biaxial testing protocols (1) and (2) are illustrated in Fig 3.3B, and C respectively.

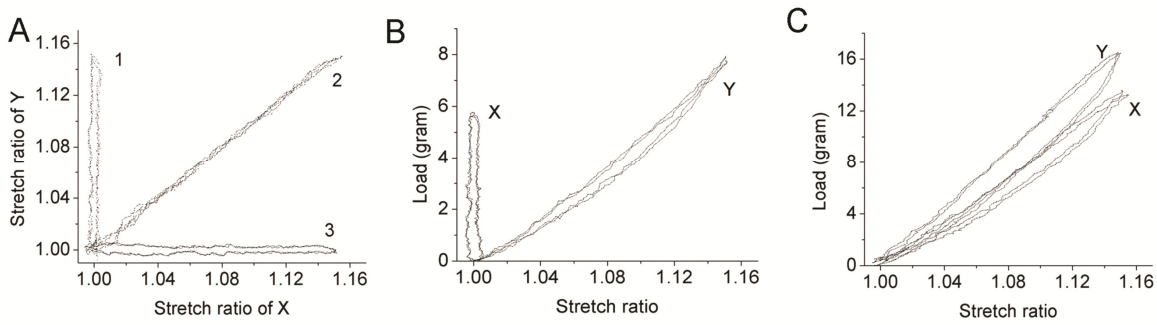

Fig 3. 3 (A) Illustrative stretch history during three separate protocols: 1. Y direction strip-biaxial stretch. 2. Equibiaxial stretch. 3. X direction strip-biaxial stretch. (B) Illustrative load-stretch data during a Y direction strip-biaxial test (curve 1 in panel A). (C) Illustrative load-stretch data during an equibiaxial stretching test (curve 2 in panel A).

3.2.2 On-line thickness measurements

Representative images of construct cross-section at select stretch ratios are shown in Figs 3.4A-D. Thicknesses obtained from OCT images were averaged and are shown in Figs 3.4E as a function of stretch ratio. Construct stretched thicknesses exhibited considerable deviation from the incompressible limit (i.e., $\lambda_3 = 1/\lambda_1\lambda_2$ where 3 is the out of plane or z direction), which is shown as reference (dotted line).

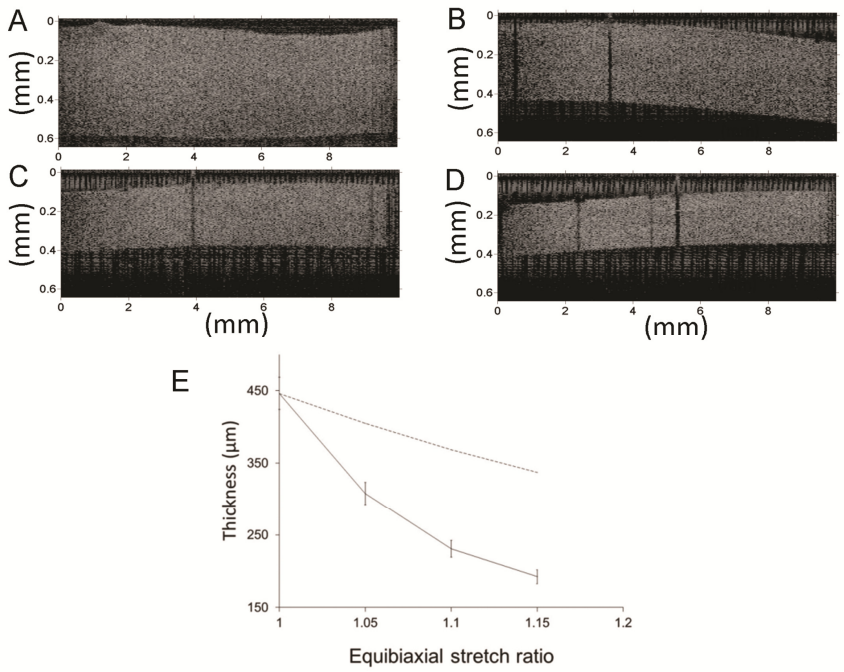

Fig 3. 4 Measurement of OCT gel thickness in situ of unstretched (A) as well as 5% (B), 10% (C), and 15% (D) equibiaxially stretched gels. Thickness is plotted as a function of equibiaxial stretch ratio, with the incompressible limit shown (dashed line) as reference (E).

3.2.3 Stress calculation

Though 'load (g)' is an important measure of mechanical responses, stress is a preferred derived quantity that can reveal tissue mechanical properties such as stiffness. Two definitions of stress are particularly useful: the first Piola-Kirchhoff (or nominal) and the Cauchy (or true) stress. The former is useful experimentally and the latter is useful analytically. The first Piola-Kirchhoff stress, P, is the measured stretch force on an unstretched area, is therefore, convenient to measure. Assuming that loads are transferred uniformly to the central region of the cruciform-shaped gel, the first Piola-Kirchhoff stress is given by the following equations [82, 83]

$$P_{11}^{central} = \frac{f_1}{L_2 H}, \qquad P_{22}^{central} = \frac{f_2}{L_1 H},$$

where f_1 and f_2 are measured applied loads in the x -y directions, and H are the thickness of the central region in the undeformed state over which the loads act (here, L_1=L_2≈ 2 cm), and H is the original thickness (~460 μm). Cauchy stress, t, is a measure of applied force acting on a current deformed area.

If one can assume incompressibility during transient loading, which holds for many mature native tissues, calculation of Cauchy stress is straight-forward. In tissue engineered constructs, especially at the beginning. Varying of mechanical stress primarily comes from water movement and the realignment of the fiber architecture, the tissues act far from incompressible during mechanical testing. Calculation of Cauchy stress, t, in planar samples also requires the more problematic on-line measurement of tissue thickness at different time points of tests , which may evolve due to cell-induced compaction or change with load-induced stretch. In the compressible regime, Cauchy stress may be calculated as,

$$t_{11}^{central} = \frac{f_1}{\lambda_2 L_2 h}, \qquad t_{22}^{central} = \frac{f_2}{\lambda_1 L_1 h},$$

Where λ_1 and λ_2 are stretch ratios, and h is current deformed thickness inferred from OCT images. Thus, current deformed thickness, h, is an important experimental parameter, yet difficult to measure particularly of soft tissue constructs in sealed bioreactors, combining load-stretch data from testing with construct thickness from

OCT, Cauchy stress is shown as a function of stretch from equibiaxial stretching tests in Fig 3.5A. Fitting plots shown in Fig 3.6B were also obtained for data analysis.

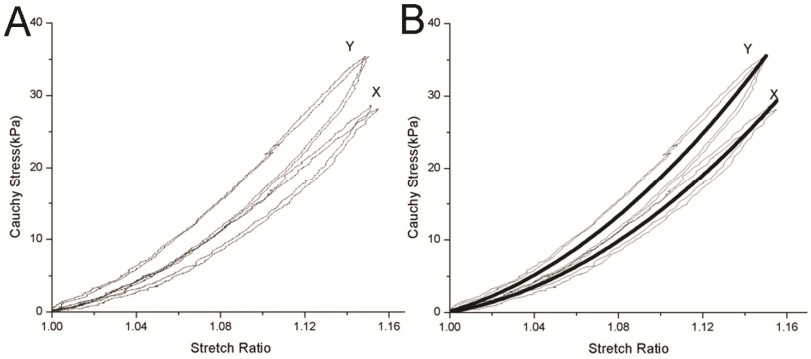

Fig 3. 5 Data process for measured stress- stretch curve. (A) stress-stretch curves calculated from thickness measurement and load-stretch data. (B) fitting the stress-stretch data with exponential curves.

3.3 Discussion

Due to high compliance and low strength etc, simple and sensitive tests or other similar way [84, 85] have often been employed to describe the mechanical responses of engineered tissues. However mechanical anisotropy of tissues complicated uniaxial data analysis for constitutive equations. Biaxial tests provide more complete data in terms of stress and strain matrices, which would better quantify the mechanical properties of engineered tissues as well as native tissues and promise to increase insight into mechanical-stimulated growth and remolding of tissues. Here, illustrative results demonstrated that three mechanical testing protocols were performed on a single construct sequentially; each protocol ran two cycles with repeatable and stable results that allowed large variations. This implied a sensitive and robust tracking mechanical

testing system, sufficient to compare responses from multiple combinations of multi-axial stress and strain, including evolving orientations of subsequently synthesized collagen.

Although applied loads are easily obtained from standard transducers, the calculation of stress from measured loads is not as straightforward. Stress is defined as applied force acting on an undeformed (the first Piola-Kirchhoff stress) or current deformed (the Cauchy stress) oriented area. Measurement of engineered tissue construct thickness emerges as a significant challenge, particularly if it is to be measured serially during an extended experimental protocol. For incompressible or nearly incompressible materials, thickness of constructs under mechanical testing may be predicted easily. However, for soft engineered tissue, especially at early stages, the solid fraction of fibers is low and the fluid volume fraction is high, thus resulting in high porosity and compressibility. Considerable deviation from the incompressible limit (Fig 3.5) implied that on-line measurement of thickness was necessary to obtain "true" stress as a function of stretch. Several methods have been reported to measure thickness, typically at the end of an experiment in conjunction with biochemical and ultrastructural analyses. These methods have included the use of a low force probe [47] or laser displacement system in which a small reflective disk was placed onto the sample and its height recorded.[86] Longitudinal measures of tissue construct thickness have included common bright field microscopy, which suffers from poor resolution especially for measuring changes in thickness of tens to hundreds of micrometers. More recently, multiphoton microscopy has been used within a biaxial device to measure thickness on native tissues, non-

invasively, using SHG in collagen as employed here. [28] The shortcomings of this approach include a limited depth of imaging with which to measure thickness, especially of dense, highly scattering tissues and, for non-invasive imaging, sole reliance on endogenous nonlinear optical signals which are inherently weak. We attempted to address these issues by incorporating coherence gated microscopy and tomography (OCM/OCT). Thus, with multimodal (NLOM-OCM) microscopy, our current system probed deeper and measured thick specimens (up to 2 mm) whose predominant components (particularly fibrin) may not have nonlinear susceptibilities that generate observable nonlinear optical signals.

CHAPTER IV

CHARACTERIZATION OF ENGINEERED CONSTRUCTS

With the aid of a custom biaxial bioreactor, NLOM-OCM was used to image collagen deposition within NHDF seeded, cruciform shaped fibrin matrices cultured under different mechanical environments namely, anchored (1.0:1.0 stretch ratio) and strip biaxial (1.0:1.1). NLOM-OCM images were obtained from the gel over 31 days. The evolving bulk properties were also quantified by intermittent mechanical testing.

4.1 Engineered constructs in culture

4.1.1 Constructs preparation

Pure fibrin gel as primary scaffold: fibrin gels were prepared in accord with established protocols.[59, 83, 89] Bovine fibrinogen (Sigma-Aldrich) was dissolved as 5 mg/ml and supplemented with e-amino caproic acid (e-ACA; Sigma), which inhibits plasmin activity that degrades fibrin. Fibrinogen solution was filtered and mixed with 5% fetal bovine serum (FBS) and thrombin (25 U/ml; Sigma) at a ratio of 1:0.002:0.002, and mixed thoroughly with cell suspension and with black polyethylene microspheres(Cospheric), which was used as fiducial markers for mechanical testing. The final densities of fibrin and cells were 10 mg/ml, 1×10^6/ml.

The solution was poured into cruciform shaped silicon rubber molds (end-to-end with variable length and arm width of 20 mm) of different sizes placed within a glass Petri dish. Customized bars of porous polyethylene (Small Parts), each punctured with two holes were positioned in the cruciform mold before adding solutions. Solutions were

left undisturbed in a humidified CO2 incubator at 37^{o}C before the mold was removed and the gel coupled to the bioreactor.

4.1.2 Static mechanical stimuli:

Cruciform-shaped gels were clamped via bars, and stretched with various ratio as shown in Fig 2.4.

4.2 Microstructural imaging and mechanical testing results

A polycarbonate lid fitted with a window assembly was used for in culture microscopic imaging (Fig 3.2). The lids were secured on the bioreactor by screws and switched under aseptic conditions in a class II biosafety cabinet. Through the imaging window, the central region of the sample was imaged at three locations. For mechanical testing, bioreactor was configured with lid containing optical window sealed as view-port to digitally record embedded fiducial markers with CCD camera. Prior to testing, constructs were preconditioned through 3 cycles of 10% biaxial stretch. With computer controlled stepper motors, tissue constructs were subjected to diverse biaxial testing protocols.

After mechanical testing, construct thicknesses were measured at different stretch ratios from cross-sectional images acquired by OCT. For thickness measurements, tissue construct was stretched within testing rig, locked in deformed configuration by set screws on load arms, transferred to microscopy stage for OCT imaging, replaced on mechanical testing rig and returned to original configuration before stretched for next OCT measurement.

4.3 Results

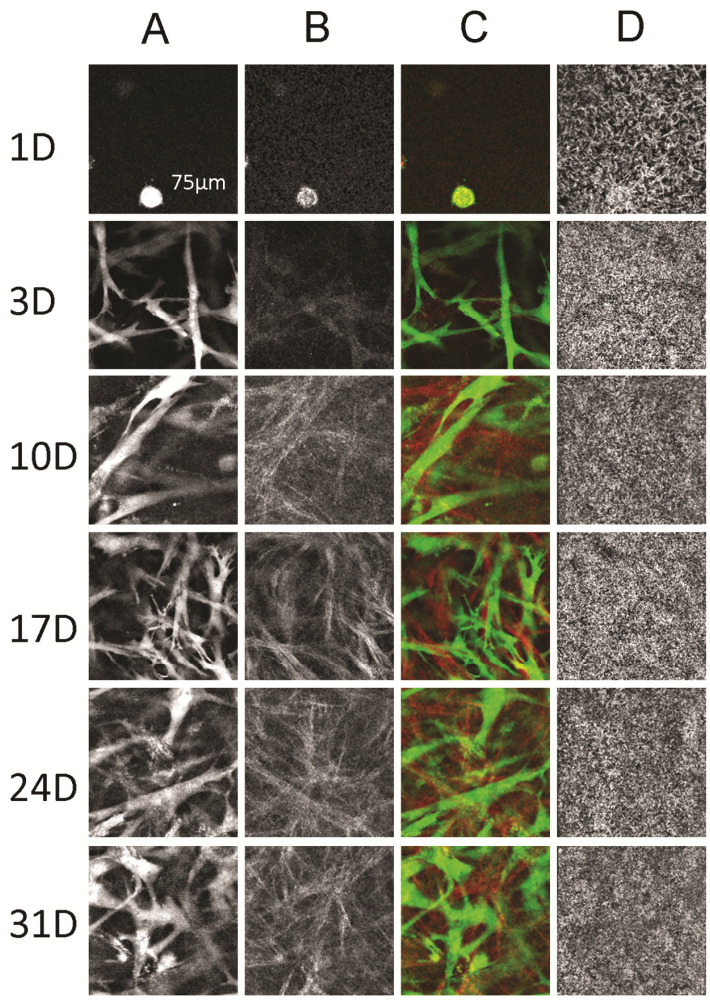

Fig 4. 1 Representative NLOM-OCM images of fibroblasts seeded in fibrin gel with 1:1 stretch ratio on day 1, 3, 10, 17, 24 and 31. (A) Cellular fluorescence by TPF. (B) SHG in collagen. (C) False color overlay showing collagen (red), and cell (green). (D) Nonspecific OCM image. Scale bar: 75µm.

NLOM-OCM images acquired from the central region of non-stretched constructs on day 1, 3, 10, 17, 24 and 31, are given in Fig 4.1. TPF images in Fig 4.1A showed NHDF initially round (Day 1) that by Day 3 have elongated and extended processes. Images rendered from SHG in Fig 4.1B suggested NHDF deposition of

collagen that accumulated over time. Overlay images of TPF and SHG shown in Fig 4.1C are false colored green and red, respectively. The overlay images showed the relative distribution of NHDF and deposited collagen, much of which appeared to be aligned with cell bodies. OCM images are shown in Fig 4.1D. Fibrin fiber and NHDF morphology were distinct on Day 1, but at later times, the fibrin gel has compacted such that OCM image contrast is dominated by its density.

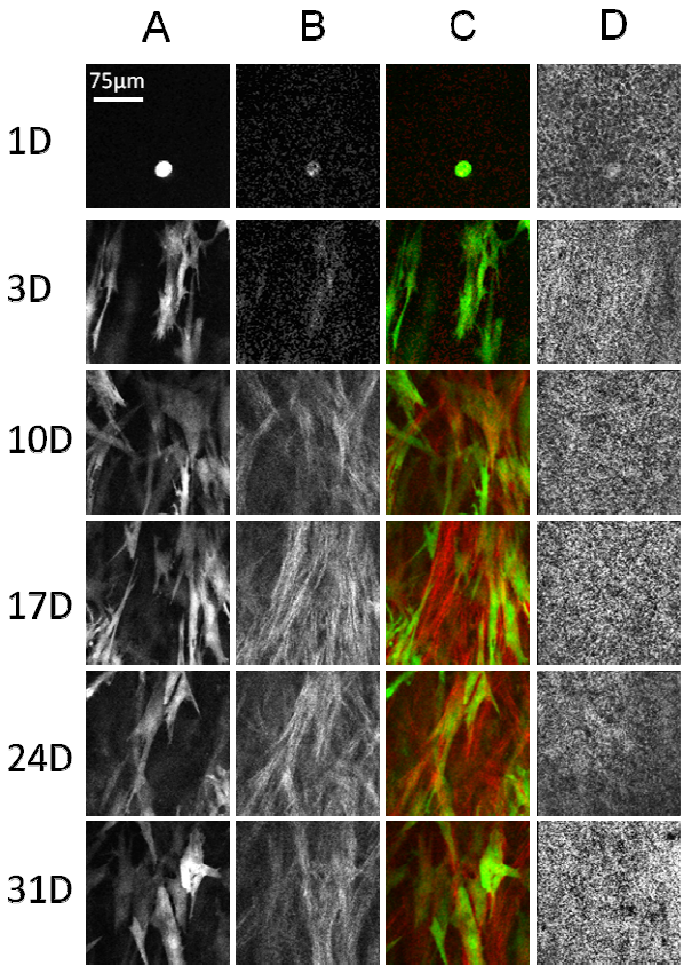

Fig 4. 2 Representative NLOM-OCM images of fibroblasts seeded in fibrin gel with 1:1.1 stretch ratio on day 1, 3, 10, 17, 24 and 31. (A) Cellular fluorescence by TPF. (B) SHG in collagen. (C) False color overlay showing collagen (red), and cell (green). (D)Nonspecific OCM image. Scale bar: 75µm.

NLOM-OCM images of engineered constructs under strip biaxial stretch (1.0:1.1 stretch ratios) are shown in Fig 4.2. The principal stretch axis is oriented vertically in the images. TPF images are shown in Fig 4.2A and, consistent with non-stretched gels, NHDF morphology was initially rounded on Day 1 and had elongated and extended processes by Day 3. Of note was that elongated cells appeared to preferentially align with principal stretch. Overlay images of TPF and SHG images shown in Fig 4.2C are false colored green and red, respectively. Consistent with anchored fibrin gels, collagen deposition appeared aligned with cell bodies, which, when cultured under strip biaxial stretch conditions, appeared preferentially aligned with principal stretch. OCM images are shown in Fig 4.2D, in which, similar to anchored fibrin gels, contrast was dominated by the dense fibrin matrix (Over the course of 24 hours, NHDF seeded fibrin gels thin from ~1 mm to ~0.1 mm, regardless of culture boundary conditions).

NLOM-OCM images from three stacks acquired from the central region of engineered constructs were analyzed to quantify evolving matrix fiber orientation. Fig 4.3 shows matrix fiber angle distributions in non-stretched (Fig 4.3A) and strip biaxial stretched constructs (Fig 4.3B). For day 1, OCM images were used to calculate fibrin fiber orientation distributions. For later time points on days 3, 10, 17, 24 and 31, SHG images were analyzed to calculate deposited collagen fiber orientation distributions; analysis of OCM images for these time points exhibited isotropic fibrin fiber angle distributions (data not shown). Early in culture, both non-stretched and stretched constructs' fibrin fibers exhibited an isotropic orientation distribution with alignment index, 1.0948 and 1.1132 respectively.

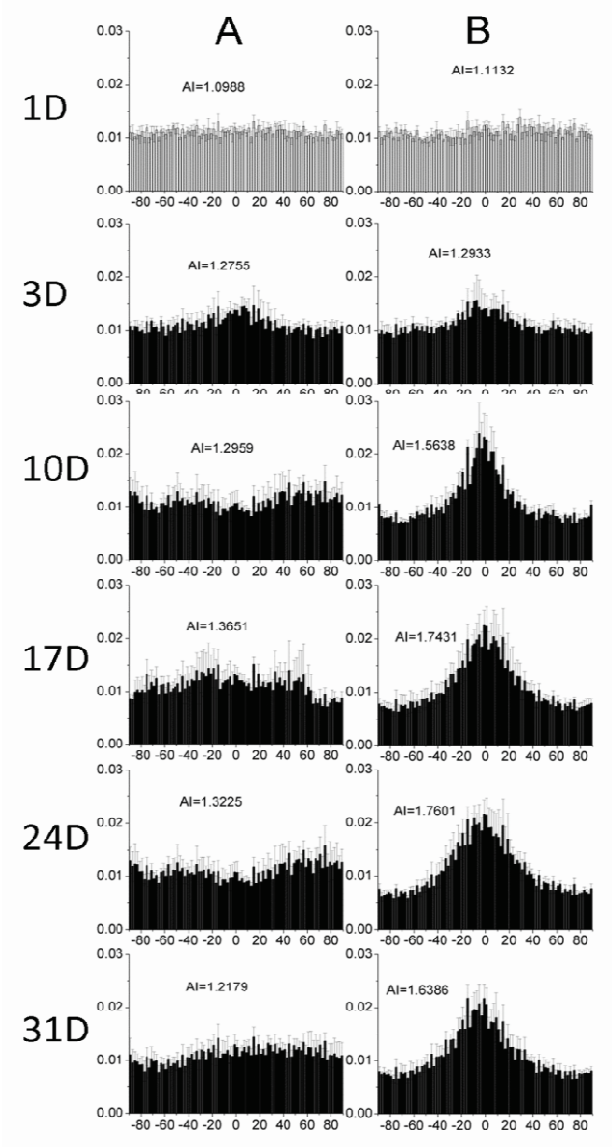

Fig 4. 3 Analyses of initial fibrin fiber on day 1 and deposited collagen fiber distribution of central region on day 3, 10, 17,24 and 31. (A). 1:1 stretch ratio. (B). 1:1.1 stretch ratio.

Yet, the principal stretch was enough to induce NHDF alignment and consequent anisotropic collagen deposition as early as Day 3 as evidenced by collagen fiber angle

distribution with AI = 1.2933 (predominant angle at 0° coincident with principal stretch axis). The collagen fiber angle distribution sharpened with culture time along the principal stretch axis with increasing AI, 1.5638, 1.7431 on days 10, 17 respectively. From day 17 to 31, AI did not show much change from 1.7431 to 1.6366. While in non-stretched gel, AI remained in relatively low, indicating isotropy. It should be noted that fibrin fiber angles exhibited isotropic distributions for each of the days (data not shown).

On the same days of imaging, constructs were also subjected to equilbiaxial mechanical testing. Cauchy stress as a function of engineering strain was obtained to quantify evolving mechanical properties. Principal stretched direction of Cauchy stress-stretch curves, performed on strip biaxial stretched constructs, is plotted in Fig 4.4.

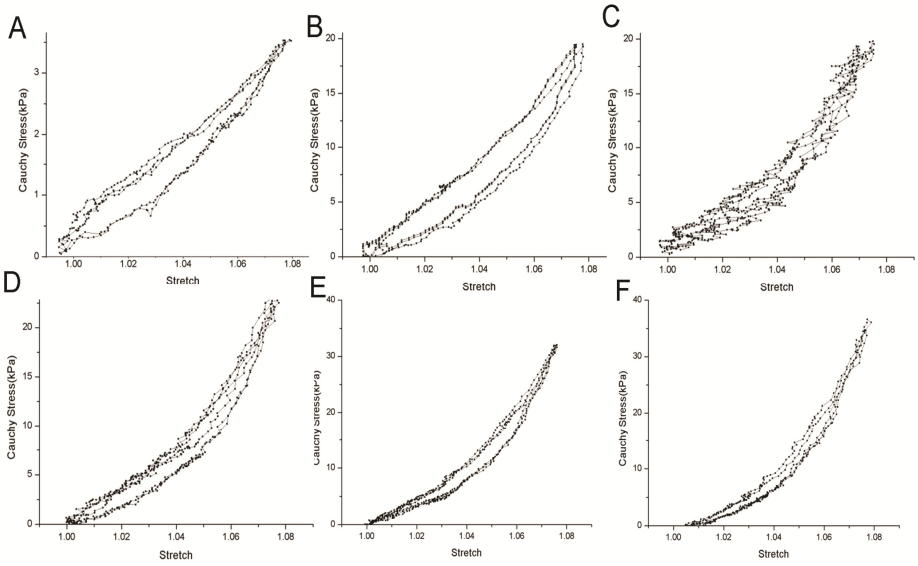

Fig 4. 4 Stress-stretch data for an engineered tissue cultured on day 3, 10, 17, 24, 31 and after cell moved on day31. (A) Day3. (B) Day 10. (C) Day 17. (D) Day 24. (E) Day 31. And (F) Day 31 after cell moved.

The mechanical response evolved from linear to non-linear stress-stretch relationships. Stress to induce 7.5% strain increased from 3 kPa on day 3 to 31 kPa on day 31, indicating an increase in load bearing. Due to hysteresis, a difference between loading and unloading curves was observed in each testing cycle.

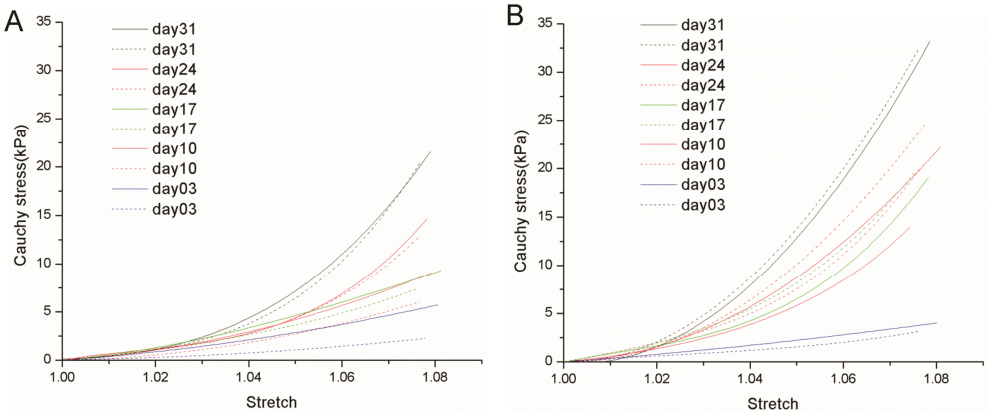

Fig 4. 5 Fitting curves of stress-strain relationship of two parallel cultured gel on day 3, 10, 17, 24 and 31. (A). 1:1 stretch ratio at the beginning. (B). 1:1.1 stretch ratio at the beginning.

Fitting plots of stress-stretch data on serial time-points are given in Fig 4.5 (Fig 4.5A refers to non-stretched, Fig 4.5B refer to stretched configuration). The peak stress achieved during mechanical testing increased significantly over the 4-week experiment under both conditions; the final stress was 4-7 times fold than the initial stress. The stress-strain curves changed from linear response to nonlinear with increasing stiffness with culture time. The differences between the stresses of vertical and horizontal directions in constructs decreased and tended to achieve comparable values through week 4. Of note is that constructs cultured under 10% strip biaxial stretch exhibited more

active growth and improved mechanical behavior than constructs without stretch stimulus.

The maximum stress induced by 7.5% stretch was 31 kPa in 10% strip biaxial stretch and 21 kPa in non-stretched constructs respectively. Strip biaxial stretch constructs showed non-linear stress-stretch behavior as early as day 10, while non-stretched constructs expressed smaller responses only after day 24.

4.4 Discussion

The characterization of evolving microstructure and properties of constructs, while maintaining sterility is a continuing challenge. In this study, force transducers were integrated into the bioreactor and sterilized before use. The bioreactor was sealed with silicone rubber gaskets and by lids. Optical access to the tissue construct within the bioreactor was facilitated by a coverslip window assembly. Microbead displacements were recorded through a sealed transparent window during mechanical testing. The chamber was sealed in sterile hood and tissues were secured in place during transfer from incubator to imaging stage and mechanical testing platform.

Many tissues, such as skin, ligaments, collagen is the main load bearing component. It is the distribution, cross-linking, and alignment of collagen, not just its mere presence, that ultimately influences overall mechanical behavior. Several strategies have been reported to produce wanted fiber alignment within engineered tissues, aimed as functional replacements of diseased or injured tissues. These strategies include magnetic forces, boundary conditions on the gels, substratum topology, and mechanical loading.[90-92] Consistent with above strategies, deposited collagen preferentially aligned

with cells in the direction of imposed principal stretch under a strip biaxial stretch condition. Due to the resolution limit of optical microscopy, both non-stretched and stretched constructs' fibrin fibers exhibited an isotropic orientation distribution. Atomic force microscopy (AFM) and Scanning electron microscopy (SEM) images with nanometer resolution, revealed fibril alignment in fribrin tissues.[92, 93] It was indicated that fibrin fibrils were reoriented with the direction of the primary strain direction.[93] Thus, in current studies, the mechanisms most likely evolve from fibrin alignment to consequent cell alignment.[94-96] Cells aligned via contact guidance to minimize distortions through their cytoskeleton by microtubules, microfilament bundles etc.[97-101]

Our study suggested, however, that the deposition of preferentially aligned collagen did not result in an overall strongly anisotropic tissue behavior. This counterintuitive result may have been a consequence of the static and, perhaps after adaptation, biaxially isotonic culture condition. Furthermore, this result may be consistent with tensional homeostasis theory, that cells tried to maintain, or restore a mechanobiological equilibrium under any configuration. A similar experiment was reported by Sander *et al* [85] in which two cruciform with differing arm widths were examined, one with a 1.0:1.0 aspect ratio and the other with 1.0:0.5 aspect ratio. Their results appeared to suggest that higher local stresses may have induced more collagen deposition, when comparing arms of different widths that ultimately homogenized local microenvironments. In addition, it was intriguing that mechanical anisotropy was observed in strip biaxially stretched tissue constructs on Day 31 only after decellularization, which suggested that the embedded cells had a homogenizing effect on

tissue mechanical properties (Fig 4.4F). A similar result was observed in tissue constructs cultured under strip biaxial stretch for much shorter duration (six days) in which collagen fiber alignment (AI) with principal stretch increased following removal of embedded fibroblasts.[48] Further work is clearly needed to define these cellular effects on matrix microscopic organization and mechanical responses.

In summary, we validated a biaxial bioreactor suitable for month long culture of cruciform shaped 3D tissue constructs that may be coupled to a multimodal NLOM-OCM system and biaxial testing platform for collecting complementary microstructural information and characterizing mechanical properties. Microscopic organization and segmentation of multi-component constructs may be characterized with NLOM-OCM as well as measurement of stretch dependent thicknesses. Mechanical properties of tissues were characterized by multiple multiaxial testing protocols. Multimodal microscopy and biaxial mechanical testing were performed longitudinally on individual engineered tissue constructs to provide time-dependent microstructural and mechanical properties. This integrated bioreactor platform enables an unprecedented opportunity to correlate evolving mechanical properties with microscopic events, including matrix deposition, initial alignment, and subsequent remodeling in mechanically stimulated tissues.

CHAPTER V

SUMMARY AND FUTURE WORK

In summary, our biaxial platform coupling NLOM-OCM with mechanical testing provided complementary microstructural information and mechanical properties. Microscopic organization and segmentation of multi-component constructs were characterized with NLOM-OCM. Thickness changing of constructs under biaxial stretch testing were measured with adapted OCT system. Mechanical properties of tissues were achieved in accurate stress-strain relations by comprehensive testing protocols. Moreover engineered tissue culture constructs under different boundary conditions were investigated during an extended experimental protocol and yielded some interesting findings. The platform enabled an unprecedented opportunity to correlate evolving mechanical properties with microscopic events, including matrix deposition, initial alignment, and subsequent remodeling in mechanically stimulated tissues.

In this study only one pair of initial stretch stimuli was compared, 1:1 with 1:1.1 ratios. To predict how engineered tissues will respond to the changes of mechanical stimuli, a more comprehensive stretch protocol need to be exerted. The next step of this research is to culture engineered tissues with more comprehensive stretch ratios, such 1.2:1.0, and 1.2:1.2. Moreover, pure fibrin gels are mimic to beginning content of wound healing, which evolves from a fibrin dominant clot to a collagen scar. [102] During the transition from the fibrin clot and a scar that is abundant in collagen, the tissues contain mainly of collagen Type III at first, then predominantly collagen Type I. Stegemann [84]

examined the gene expression of cells in collagen I, fibrin, and composite of these two. There was higher Collagen Type III expression in fibrin than in collagen-containing matrices. Expression of Collagen I and tropoelastin were higher in pure collagen and collagen-fibrin mixtures than in pure fibrin gels.

It will be our future investigation to find out if the deposition and development of collagen I would be facilitated within composite of fibrin and collagen I, compared to pure fibrin gels.

REFERENCES

1. Taber, L. A. “Biomechanics of growth, remodeling, and morphogenesis”. Appl Mech Revs 48, 487-545(1995).

2. Barocas, V. H., Tranquillo, R. T. “An anisotropic biphasic theory of tissue equivalent mechanics: the interplay among cell traction, fibrillar network deformation, fibril alignment, and cell contact guidance”. ASME J Biomech Eng 119, 137-145(1997).

3. Olsen, L., Maini, P. K., Sherratt, J. A., Callon, J. “Mathematical modeling of anisotropy in fibrous connective tissue”. Math Biosci 158, 145-170(1999).

4. Driessen, N. J. B., Peters, G. W. M., Huyghe, J. M., Bouten, C. V. C., Baaijens, F. P. T. “Remodeling of continuously distributed collagen fibres in soft connective tissues”. J Biomech 36, 1151-1158(2003).

5. Driessen, N. J. B., Wilson, W., Bouten, C. V. C., Baaijens, F. P. T. “A computational model for collagen fibre remodeling in the arterial wall”. J Theor Biol 226, 53-63(2004).

6. Barbara Brodsky, B., Ramshaw, J. A. M. “The collagen triple-helix structure”, Matrix Biology 15, 545–554 (1997).

7. Kramer, R. Z., Bella, J., Mayville, P., Brodsky, B., Berman, H. M. “Sequence dependent conformational variations of collagen triple-helical structure”. Nat Struct Biol.6, 454-457 (1999).

8.Vuorio, E., and Cromhrugghe, B. D. “The family of collagen genes”. Annu. Rev. Biochem 59, 837-872 (1990).

9. Marie-Pierre Simon, M-P., Florence Pedeutour, F.M., *et al*. “Deregulation of the platelet-derived growth factor β-chain gene via fusion with collagen gene COL1A1 in

dermatof ibrosarcoma protuberans and giant-cell fibroblastoma". Nature Genetics 15, 95 - 98 (1997).

10. Donald M. Bell, D. M., Keith K.H. Leung, K. K. H., et al. "SOX9 directly regulates the type-ll collagen gene". Nature Genetics 16, 174 - 178 (1997).

11. Kucharz, E. J. "The collagens: biochemistry and pathophysiology". Springer-Verlag, Berlin, 34-39(1992).

12. Davis, G. E., Bayless, K. J., Davis, M. J., Meininger, G. A. "Regulation of tissue injury responses by the exposure of matricryptic sites within the extracellular matrix molecules". Am J Path 156, 1489-1498(2000).

13. Duncan, M. R., Frazier, K, S., et al. "Connective tissue growth factor mediates transforming growth factor β-induced collagen synthesis: down-regulation by cAMP". The FASEB Journal 13, 1774-1786 (1999).

14. Leblond, C. P. "Synthesis and secretion of collagen by cells of connective tissue, bone, and dentin". The Anatomical Record 224, 123–138 (1989).

15. Weinstock, M., and Leblond, C. P. "Synthesis, migration, and release of precursor collagen by odontoblasts as visualized by radioautography after [3H] proline administration". JCB 60, 92-127 (1974).

16. Canty, E. G., Kadler, K. E. "Procollagen trafficking, processing and fibrillogenesis". J Cell Sci 118, 1341-1353 (2005).

17. G. J. Laurent, G. J. "Dynamic state of collagen: pathways of collagen degradation in vivo and their possible role in regulation of collagen mass". AJP-Cell Physiology 252, 1-9 (1987).

18. Cui, F-Z., Li, Y., Ge, J. “Self-assembly of mineralized collagen composites”. MS&E-R: Reports, 57, 1-27 (2007).

19. Leung, D. Y. M., Glagov, S., Matthews, M. B. “Cyclic stretching stimulates synthesis of matrix components by arterial smooth muscle cells in vitro”. Science 191, 475-477(1976).

20. MacKenna, D., Summerour, S. R., and Francisco, V. J. “Role of mechanical factors in modulating cardiac fibroblast function and extracellular matrix synthesis”. Cardiovasc Res 46, 257-263 (2000).

21. Gupta, V., and Grande-Allen, K. J. “Effects of static and cyclic loading in regulating extracellular matrix synthesis by cardiovascular cells”. Cardiovasc Res 72, 375-383 (2006).

22. Rodriguez-Feo, J. A., Sluijter, J. P. G., de Kleijn, D. P. V., Pasterkamp, G. “Modulation of collagen turnover in cardiovascular disease”. Curr Pharmacol Design 11, 2501-2514 (2005).

23. Bishop, J. E., and Laurent, G. J. “Collagen turnover and its regulation in the normal and hypertrophying heart”. Eur Heart J 16, 38-44 (1995).

24. Brilla, C. G., Zhou, G., Rupp, H., Maisch, B., Weber, K. T. “Role of angiotensin II and prostaglandin E2 in regulating cardiac fibroblast collagen turnover”. Am J Cardiol 76, 8-13 (1995).

25. Chase, A. J., Newby, A. C. “Regulation of matrix metalloproteinase (matrixin) genes in blood vessels: a multi-step recruitment model for pathological remodeling”. J Vasc Res 40, 329-343(2003).

26. Baek, S., Rajagopal, K. R., Humphrey, J. D. “A theoretical model of enlarging intracranial fusiform aneurysms”. ASME J Biomech Eng 128, 142-149(2006).

27. Eastwood, M., V. C. Mudera, D. A. McGrouther, R. A. Brown. “Effect of precise mechanical loading on fibroblast populated collagen lattices morphological changes”. Cell Motility and the Cytoskeleton 40, 13-21(1998).

28. Keyes, J. T., S. M. Borowicz, J. H. Rader, U. Utzinger, M. Azhar, J. P. Vande. “Design and demonstration of a microbiaxial optomechanical device for multiscale characterization of soft biological tissues with two-photon microscopy”. Microsc Microanal 17, 167-175(2011).

29. Voytik-Harbin, S. L., Roeder, B. A., Sturgis, J. E., Kikini, K., Robinson, J. P. “Simultaneous mechanical loading and confocal reflection microscopy for three-dimensional microbio-mechanical analysis of biomaterials and tissue constructs”. Microsc Microanal 9, 74-85(2003).

30. Raub, C.B., V. Suresh, T. Krasieva, J. Lyubovitsky, J. D. Mih, A. J. Putnam, et al. “Noninvasive assessment of collagen gel microstructure and mechanics using multiphoton microscopy”. Biophys J 92, 2212-2222(2007).

31. Raub, C.B., J. Unruh, V. Suresh, T. Krasieva, T. Lindmo, E. Gratton, et al. “Image correlation spectroscopy of multiphoton images correlates with collagen mechanical properties”. Biophys J 94, 2361-2373(2008).

32. Rho, J. Y., M. E. Roy, T.Y. Tsui, G. M. Pharr. “ Elastic properties of microstructural components of human bone tissue as measured by nanoindentation”. Journal of Biomedical Materials Research 45, 48-54(1999).

33. Prajapatic, R. T., Chavally-Mis, B., Herbage, D., Eastwood, M., Brown, R. A. "Mechanical loading regulates protease production by fibroblasts in three-dimensional collagen substrates".Wound Repair Regen 8, 226-237(2000).

34. Knezevic, V., Sim, A. J., Borg, T. K., Holmes, J. W. "Isotonic biaxial loading of fibroblast-populated collagen gels: a versatile, low-cost system for the study of mechanobiology". Biomech Model Mechanobiol 1, 59-67(2002).

35. Hartmann, A., Boukamp, P., and Friedl, P. "Confocal reflection imaging of 3D fibrin polymers". Blood Cells Mol Dis 36, 191-193(2006).

36. Hakkinen, K. M., Harunaga, J. S., Doyle, A. D., Yamada, K. M. "Direct comparisons of the morphology, migration, cell adhesions, and actin cytoskeleton of fibroblasts in four different three-dimensional extracellular matrices". Tissue Eng. Part A 17, 713–724(2011).

37. Wolf, K., Mazo, I., Leung, H., et al. "Compensationmechanism in tumor cell migration: Mesenchymal-amoeboid transition after blocking pericellular proteolysis". J. Cell Biol 160, 267–277(2003).

38. Izatt, J. A., Hee, M. R., Owen, G. M., Swanson, E. A., and Fujimoto, J. G. "Optical coherence microscopy in scattering media". Opt. Lett 19, 590–592 (1994).

39. Clark, A. L., Gillenwater, A., Alizadeh-Naderi, R., El-Naggar, A. K., and Richards-Kortum, R. "Detection and diagnosis of oral neoplasia with an optical coherence microscope". J. Biomed. Opt 9, 1271–1280 (2004).

40. Denk, W., Strickler, J. H., and Webb, W. W. "Two-photon laser scanning fluorescence microscopy". Science 248, 73-76(1990).

41. Campagnola, P. J., Millard, A. C., Terasaki, M. P., Hoppe, E. C., Malone, J., and Mohler, W. A. “Three-dimensional high-resolution second harmonic generation imaging of endogenous structural proteins in biological tissues”. Biophys. J. 82 (1 Pt 1), 493–508(2002).

42. Guo, Y., Ho, P., Savage, H., Harris, D., Sacks, P., Schantz, S., Liu, F., et al. “Second-harmonic tomography of tissues”. Opt. Lett 22, 1323-1325(1997).

43. Cheng, J., Book, L. D., and Xie, X. S. “Polarization coherent anti-Stokes Raman scattering microscopy”. Opt. Lett 26, 1341-1343(2001).

44. Potma, E. O., de Boeij, W. P., Haastert, P. J. M., and Wiersma, D. A. “Real-time visualization of intracellular hydrodynamics in single living cells”. Proc. Nat. Acad. Sci. USA 98, 1577-1582(2001).

45. Sacks, M. S. “Incorporation of experimentally-derived fiber orientation into a structural constitutive model for planar collagenous tissues”. ASME J Biomech Eng 125, 280-287(2003).

46. Wells, P. B., Yeh, A. T., Humphrey, J. D. “Influence of glycerol on the mechanical reversibility and thermal damage susceptibility of collagenous tissue”. IEEE Trans Biomed Eng 53, 747-753(2006).

47. Hall, H., T. Baechi, and J. A. Hubbell. “Molecular properties of fibrin-based matrices for promotion of angiogenesis in vitro”. Microvasc Res 62, 315-326(2001).

48. Hu, J., Humphrey, J. D., and Yeh, A. T. “Characterization of Engineered Tissue Development Under Biaxial Stretch Using Nonlinear Optical Microscopy”. Tissue Engineering Part A 15, 1553-1564(2009).

49. Niklason, L. E., Yeh, A.T., Calle, E.A., Bai, Y., Valentin, A., and Humphrey, J.D. "Enabling tools for engineering collagenous tissues integrating bioreactors, intravital imaging, and biomechanical modeling". Proc. Natl Acad. Sci. USA 107, 3335-3339(2010).

50. Tan, W., Vinegoni, C., Norman, J. J., Desai, T.A., and Boppart, S. A. "Imaging cellular responses to mechanical stimuli within three-dimensional tissue constructs". Microsc Res Tech 70, 361-371(2007).

51. Gleason, R. L., Grey, S., Wilson, E., Humphrey, J. D. "A multiaxial computer-controlled organ culture and biomechanical device for mouse carotid arteries". ASME J Biomech Eng 126, 787-795(2004).

52. Atala, A. "Tissue engineering, stem cells and cloning: Current concepts and changing trends". Expert Opin Biol Ther 5, 879-892(2005).

53. Atala, A. "Tissue engineering and regenerative medicine: Concepts for clinical application". Rejuvenation Res 7, 15-31(2004).

54. Badylak, S. F. "Xenogeneic extracellular matrix as a scaffold for tissue reconstruction". Transpl Immunol 12, 367-377(2004).

55. Vorp, D., Maul, T., Nieponice, A. "Molecular aspects of vascular tissue engineering". Front Biosci 10, 768-789(2005).

56. Niklason, L. E., Langer, R. S. "Advances in tissue engineering of blood vessels and other tissues". Transpl Immunol 5, 303-306(1997).

57. McKee, J. A., Banik, S. S., Boyer, M. J., Hamad, N. M., Lawson, J. H., Niklason, L. E., Counter, C. M. "Human arteries engineered in vitro". EMBO Rep 4, 633-638(2003).

58. Collins, K., Mitchell, J. R. “Telomerase in the human organism”. Oncogene 21, 564-579(2002).

59. Thie, M., Schlumberger, W., Semich, R., Rauterberg, J., and Robenek, H. “Aortic smooth muscle cells in collagen lattice culture: effects on ultrastructure, proliferation and collagen synthesis”. Eur J Cell Biol 55, 295-304(1991).

60. Clark, R. A., Nielsen, L. D., Welch, M. P., and McPherson, J. M. “Collagen matrices attenuate the collagen-synthetic response of cultured fibroblasts to TGF-β”. J Cell Sci 108, 1251-1261(1995).

61. Rassl, E. D., Oegema, T. R., Tranquillo, R. T. “Fibrin as an alternative biopolymer to type-I collagen for the fabrication of a media equivalent”. J Biomed Mater Res. 60, 607-612(2002).

62. Neidert, M. R., Lee, E. S., Oegema, T. R., Tranquillo, R. T. “Enhanced fibrin remodeling in vitro with TGF-beta1, insulin and plasmin for improved tissue-quivalents”. Biomaterials 23, 3717-3731(2002).

63. Long, J. L. and Tranquillo, R. T. “Elastic fiber production in cardiovascular tissue equivalents”. Matrix Biol Voume 22, 339-350(2003).

64. Cukierman, E., Pankov, R., Stevens, D. R., and Yamada, K. M. “Taking cell-matrix adhesions to the third dimension”. Science 294, 1708–1712 (2001).

65. Rhee, S., and Grinnell, F. “Fibroblast mechanics in 3D collagen matrices”. Adv Drug Deliv Rev 59, 1299-1305(2007).

66. Sandulache, V. C., Parekh, A., Dohar, J. E., and Hebda, P. A. “Fetal dermal fibroblasts retain a hyperactive migratory and contractile phenotype under 2-and 3-

dimensional constraints compared to normal adult fibroblasts". Tissue Eng 13, 2791-2801(2007).

67. Karamichos, D., Brown, R. A., and Mudera, V. "Complex dependence of substrate stiffness and serum concentration on cell-force generation". J Biomed Mater Res A 78, 407-415(2006).

68. Maaser, K., Wolf, K., Klein, C. E., Niggemann, B., Zanker, K. S., Brocker, E. B., and Friedl, P. "Functional hierarchy of simultaneously expressed adhesion receptors: integrin alpha2beta1but not CD44 mediates MV3 melanoma cell migration and matrix reorganization within three-dimensional hyaluronancontaining collagen matrices". Mol Biol Cell 10, 3067-3079(1999).

69. Grinnell, F., and Petroll, W.M. "Cell motility and mechanics in three-dimensional collagen matrices". Annu Rev Cell Dev Biol 26, 335-361(2010).

70. Cukierman, E., Pankov, R., Stevens, D. R., and Yamada, K. M. "Taking cell-matrix adhesions to the third dimension". Science 294, 1708-1712(2001).

71. Cukierman, E., Pankov, R., and Yamada, K. M. "Cell interactions with three-dimensional matrices". Curr Opin Cell Biol 14, 633-640(2002).

72. Sun, T., Haycock, J., and Macneil, S. "In situ image analysis of interactions between normal human keratinocytes and fibroblasts cultured in three-dimensional fibrin gels". Biomaterials 27, 3459-3465(2006).

73. Radisky, D. C., Levy, D. D., Littlepage, L. E., Liu, H., Nelson, C. M., Fata, J. E., et al. "Rac1b and reactive oxygen species mediate MMP-3-induced EMT and genomic instability". Nature 436, 123-127(2005).

74. Thie, M., Schlumberger, W., Semich, R., Rauterberg, J., and Robenek, H. “Aortic smooth muscle cells in collagen lattice culture: effects on ultrastructure, proliferation and collagen synthesis”. Eur J Cell Biol 55, 295-304(1991).

75. Tang, S., Krasieva, T. B., Chen, Z., and Tromberg, B. J. “Combined multiphoton microscopy and optical coherence tomography using a 12-fs broadband source”. J. Biomed. Opt. 11, 020502 (2006).

76. Moreaux, L., Sandre, O., Blanchard-Desce, M., and Mertz, J. “Membrane imaging by simultaneous second-harmonic generation and two-photon microscopy”. Opt. Lett. 25, 320-322 (2000).

77. Brown, R. A., R. Prajapati, D. A. McGrouther, I. V. Yannas, M. Eastwood. “Tensional homeostasis in dermal fibroblasts: mechanical responses to mechanical loading in three-dimensional substrates”. J. Cell. Physiol 175, 323-332(1997).

78. Butler, D. L., S. A. Goldstein, and F. Guilak. “Functional tissue engineering: the role of biomechanics”. J. Biomech. Eng 122, 570-575(2000).

79. Pizzo, A.M., K. L. Kokini, C. B. Vaughn, Z. Waisner, S. L. Voytik-Harbin. “Extracellular (ECM) microstructural composition regulates local cell-ECM biomechanics and fundamental fibroblast behavior: a multidimensional perspective”. J Appl Physiol 98, 1909-1921(2005).

80. Humphrey, J. D., P. Wells, S. Baek, J. Hu, K. McLeroy, and A. T. Yeh. “A theoretically-motivated biaxial tissue culture system with intravital microscopy”. Biomechanics and Modeling in Mechanobiology 7, 323-334(2008).

81. De Boer, J. F., B. Cense, B. H. Park, M. C. Pierce, G. J. Tearney, and B. E. Bouma. "Improved signal-to-noise ratio in spectral-domain compared with time-domain optical coherence tomography". Opt. Lett. 28, 2067-2069(2003).

82. Humphrey, J. D., R. K. Strumpf, and F. C. Yin. "Biaxial Mechanical Behavior of Excised Ventricular Epicardium". Am. J. Physiol 259, 101-108(1990).

83. Humphrey, J. D. "Cardiovascular solid mechanics – Cells, tissues and organs", Chapter 3-5. New York, Springer(2002).

84. Hong H. and J. P. Stegemann. "2D and 3D collagen and fibrin biopolymers promote specific ECM and integrin gene expression by vascular smooth muscle cells". J Biomater Sci Polym Ed. 19, 1279-1293 (2008).

85. Sander, E. A., V. H. Barocas, and R. T. Tranquillo. "Initial Fiber Alignment Pattern Alters Extracellular Matrix Synthesis in Fibroblast-Populated Fibrin Gel Cruciforms and Correlates with Predicted Tension". Ann. Biomed. Eng 39, 714-729(2010).

86. Balestrini, J. L. and K. L. Billiar. "Equibiaxial cyclic stretch stimulates fibroblasts to rapidly remodel fibrin". J. Biochem 39, 2983-2990(2006).

87. Stegemann, H., and Stalder, K. "Determination of hydroxyproline". Clin. Chim. Acta. 18, 267-273(1967).

88. Young, J. W., Locke, J. C., Alphan, A., Rosenfeld, N., et al. "Measuring single-cell gene expression dynamics in bacteria using fluorescence time-lapse microscopy". Nature Protocols 7, 80–88 (2012).

89. Baker, M. "Cellular imaging: Taking a long, hard look". Nature 466, 1137–1140 (2010).

90. Tranquillo, R. T., Girton, T. S., Bromberek, B. A., Triebes, T. G., Mooradian, D. L. "Magnetically orientated tissue-equivalent tubes: application to a circumferentially orientated media-equivalent". Biomaterials 17, 349–357(1996).

91. Costa, K. D., Lee, E. J., Holmes, J. W. "Creating alignment and anisotropy in engineered heart tissue: role of boundary conditions in a model three-dimensional culture system". Tissue Engineering 9, 567–577(2003).

92. Sander, E., Barocas, V., Tranquillo, R. T. "Initial fiber alignment pattern alters extracellular matrix synthesis in fibroblast-populated fibrin gel cruciforms and correlates with predicted tension". Ann Biomed Eng 39, 714-729 (2010).

93. Matsumoto, T., Sasaki, J., Alsberg, E., Egusa, H., Yatani, H.& Sohmura, T. "Three-dimensional cell and tissue patterning in a strained fibrin gel system". PLoS ONE 2, e1211(2007).

94. Barocas, V. H., and Tranquillo, R. T. "An anisotropic biphasic theory of tissue-equivalent mechanics: the interplay among cell traction, fibrillar network deformation, fibril alignment, and cell contact guidance". J. Biomech. Eng 119, 137–146 (1997).

95. Oshumi, T. K., Flaherty, J. E. , Evans, M. C., and Barocas, V. H. "Three-dimensional simulation of anisotropic cell driven compaction". Biomech. Model. Mechanobiol 7, 53–62 (2008).

96. Tranquillo, R. T. "Self-organization of tissue equivalents: the nature and role of contact guidance". Biochem. Soc. Symp 65, 27–42 (1999).

97. Curtis, A. S. G., and Clark, P. "The effects of topographic and mechanical properties of materials on cell behavior". Critical Reviews in Biocompatibility 5, 343-362 (1990).

98. Oakley, C., and Brunette, D. M. “The sequence of alignment of microtubules, focal contacts and actin filaments in fibroblasts spreading on smooth and grooved titanium substrata”. Journal of Cell Science 106, 343-354 (1993).

99. Bollard, T. D., Blanchoin, L., and Mullins, R. D. “Molecular mechanism controlling actin filament dynamics in nonmuscle cells”. Annu. Rev. Biophys. Biomol. Struct 29, 545–576 (2000).

100. Helfand, B. T., Chang, L., and Goldman, R. D. “The dynamic and motile properties of intermediate filaments” . Annu. Rev. Cell Dev. Biol 19, 445–467 (2003).

101. N´ed´elec, F., Surrey, T., and Karsenti, E. “Self-organisation and forces in the microtubule cytoskeleton”. Curr. Opin. Cell Biol 15, 118–124 (2003).

102. Martin, P. “Wound healing — aiming for perfect skin regeneration”. Science 276, 75–81(1997).

103. Freund, I., Deutsch, M., Sprecher, A. “Connective-tissue polarity - optical 2nd harmonic microscopy, crossed-beam summation, and small-angle scattering in rat-tail tendon”. Biophys J 50, 693-712 (1986).

104. Drexler, W., Morgner, U., Kartner, F. X., Pitris, C., Boppart, S. A., Li, X. D., Ippen, E. P., and Fujimoto, J. G. "In vivo ultrahigh-resolution optical coherence tomography" Optics Letters 24, 1221-1223 (1999).

105. Izatt, J. A., Kulkarni, M. D., Wang, H. W., Kobayashi, K., and Sivak, M. V. "Optical coherence tomography and microscopy in gastrointestinal tissues" Ieee Journal of Selected Topics in Quantum Electronics 2, 1017-1028 (1996).

106. Schmitt, J. M. "Optical coherence tomography (OCT): A review", Ieee Journal of Selected Topics in Quantum Electronics 5, 1205-1215 (1999).

107. Wu, Q. F., Applegate, B. E. and Yeh, A. T. "Cornea microstructure and mechanical responses measured with nonlinear optical and optical coherence microscopy using sub-10-fs pulses", Biomedical Optics Express 2, 1135-1146 (2011).

108. Larson, A. M., Lee, A., Lee, P. F., Bayless, K. J., and Yeh, A. T. "Ultrashort pulse multispectral non-linear optical microscopy", Journal of Innovative Optical Health Sciences 2, 27-35 (2009).

APPENDIX A

MULTIMODAL OPTICAL MICROSCOPY

Ultrashort pulses provide the unique capabilities of simultaneous excitation of a broad range of fluorophores and a short coherence gate for high-resolution optical coherence microscopy of tissues or deposited scattering precipitates. Different optical microscopy techniques have been widely used in biomedical research with the advantages of non-invasive, high speed, and high resolution imaging of structure and biological information of the sample. Combination of different imaging modalities provided complementary information of the sample. In this study, a integrated system based on sub-10-fs was developed. Nonlinear optical microscopy (NLOM) uses the nonlinear signals from the sample normally generated by femtosecond laser pulses to provide 3-dimentional (3D) imaging of thick biological tissue and live animals.

The most common nonlinear signals used in biomedical research are multi-photon excited fluorescence, harmonic generation, and coherent anti- Stokes Raman scattering. Two-photon excited fluorescence and second harmonic generation were implemented on the same setup and used in our NLOM system to simultaneously image both the cells and collagen structure in tissue, respectively. The SHG energy-level diagram [103] was visualized in Fig A. 1.

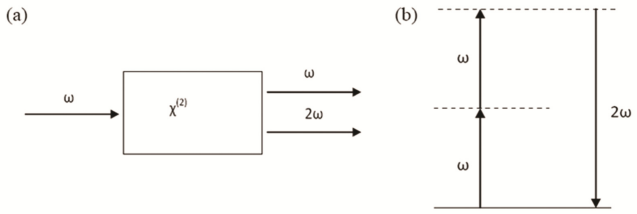

Fig A. 1 SHG excitation processes

During the relaxation of the excited state in TPF (Fig A.2), some of the incident light energy is lost. Due to the energy conserving, the emitting photon in SGH is exactly twice the energy of the incident photon.

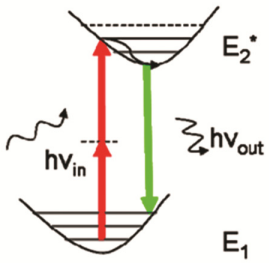

Fig A. 2 Two-photon excitation processes.

SHG has several advantages in biomedical imaging. Since there is no excitation of molecules in this process, there is no photo-bleaching or photo-toxicity from the sample. Also since SHG is normally generated from the intrinsic structure of the sample, there is no need to label the sample with exogenous fluorescence probes. In SHG imaging, near-infrared light is normally used, which can increase the penetration depth in biological tissue. Two-photon microscopy has become a popular technology in fluorescence imaging of biological thick tissue and live animals.

The benefits of utilizing the short coherence length of ultrashort pulses to improve axial resolution of OCT/M are well known. [104] Using Fourier-domain detection, the frequency components of the interferogram produced by the sample and reference arms encode the spatial profile of the biological sample along the optical axis (A-line) within the confocal parameter of the imaging objective. [105] Rapid imaging can be achieved by scanning this A-line across the sample in two dimensions. Thus, for OCT imaging a low numerical aperture (NA) objective resulting in a large depth of field is desirable, so long as the diffraction-limited lateral resolution remains comparable to the axial resolution, [105, 106] Δz, which depends on the source frequency bandwidth at full-width-half-maximum (FWHM) as below:

$$\Delta z = \frac{2(\ln 2)}{\pi} \frac{\lambda_0^2}{\Delta\lambda}$$

Our sub-10-fs pulses have a theoretical axial resolution of 2.12 μm. This resolution is significant when imaging individual cells and small-scale tissue structures in developing constructs. In the context of combining OCM with NLOM, the resolution offered by use of ultrashort pulses also better matches the NLOM interaction volume resulting from a tightly focusing high NA objective so simultaneously acquired NLOM and OCM images are co-registered. [107]

Our multimodal optical system,as shown in Fig 2.1, combined NLOM and Fourier-domain OCT/M in a single platform. Detailed more in these reports [107, 108], we describe the instrument here briefly. Sub-10-fs pulses were dispersion compensated using double chirped mirrors (GSM 270, Femtolasers) and coupled to the multi-modal

imaging system. For combined NLOM-OCM, a 5% beamsplitter splited the beam into signal and reference arms in a Michelson interferometer configuration. The signal arm was coupled by galvanometer mirrors (Cambridge Technology, Cambridge, MA), directed into an upright microscope (Axioskop2, MAT, Carl Zeiss, Thornwood, NY) equipped with the water-immersion imaging objective (20X, 1.0 NA or 40X, 0.8 NA, Carl Zeiss) which focused the pulses to a diffraction-limited spot that was scanned laterally. Backscattered laser light from the sample was combined with the return beam of the reference arm and directed to a custom spectrometer for Fourier-domain OCM. The custom spectrometer includes reflective grating (1200 lines/mm), collimating lens and CCD array (Basler, Exton, PA). Dispersion was matched in the reference arm using a combination of a prism pair and BK7 glass. For OCM, the interferogram obtained from each pixel was integrated into a single intensity value to build up a 256 x 256 2-D image rendered *en face*. Simultaneously, NLOM signals were detected by PMT detectors (Hammamatsu, Bridgewater, NJ) by appropriate dichroic mirrors and bandpass filters (Chroma). Photon counts were saved as intensity values.

The OCM in this study used a Fourier domain detection scheme in which a spectrometer was built to detect the spectrum of the OCM signal. To achieve the best result, system design software ZEMAX (ZEMAX, Bellevue, WA) was used to simulate the spectrometer design and the spectrometer was built accordingly. Figure A.3 showed the 3D layout of the spectrometer design in ZEMAX simulation. 5 wavelengths from 700 nm to 900 nm with 50nm space which cover most of the spectrum of our laser were used to simulate the whole spectrum of the laser source. The light coming out of the

single mode fiber is simulated as a point source with 0.13 NA aperture, which is same as the NA of the fiber. The beam is then collimated using an achromat and dispersed by a diffraction grating. A triple lens design was then used to focus the dispersed spectrum of the beam onto a CCD camera (L104k-2k, Basler, Exton, PA).

Since camera used has a pixel size of 10 μm by 10 μm with a total of 2048 pixels, to best use the CCD sensor the whole spectrum needs to be focused to about 20 mm in length. The spot diagram from ZEMAX for the spectrum range 700 – 900 nm the focused length is 19 mm, which is very close to the sensor size. To make sure there is no cross-talk at adjacent pixels on the CCD sensor, the Huygens PSF cross section at the focus is calculated. The spectrometer was calibrated after setup by an argon lamp (6030, Oriel, Stratford, CT) with known spectrum.

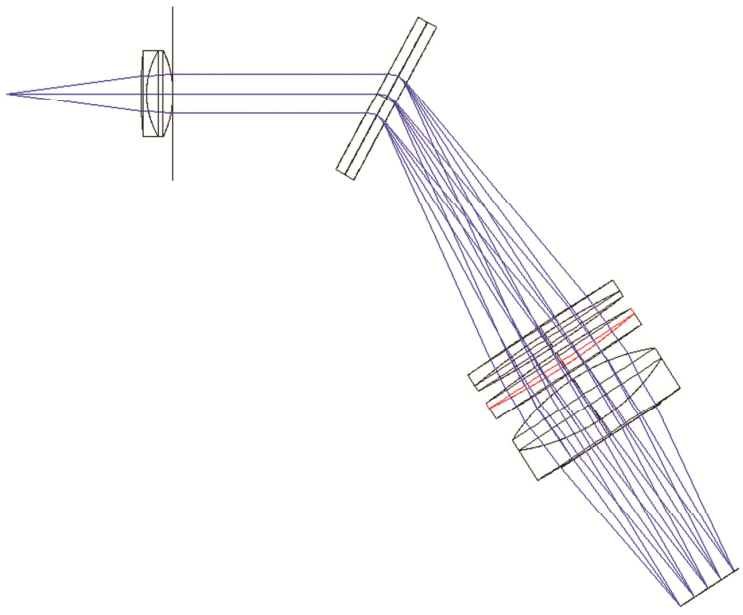

Fig A. 3 Layout of spectrometer design in ZEMAX simulation.

.

APPENDIX B

PROTOCOL FOR PREPARING FIBRIN-COLLAGEN MIXTURE WITH CELL

Preparation of components:

- Fetal bovine serum (FBS, Atlanta S12450).
- Phosphate buffered saline (PBS, Sigma P4417), dissolved in distilled water. filtered by 0.22 μm and stored in room temperature.
- Albumin from bovine plasma (BSA, Sigma A9418).
- ϵ-amino caprocis acid (ϵ-ACA, Acros A0270582), dissolved in distilled water as 100mg/ml, filtered by 0.22 μm and stored in room temperature.
- Thrombine from bovine plasma (Sigma T6634), solution are diluted in 50unit/ml in 1%BSA in PBS, stored in -20 ^{0}C degree.
- Fibrinogen from bovine plasma (Sigma F8630)
- 0.1M $Cacl_2$ solution (Sigma C5670)
- Collagen Type I (Rat tail high concentration at 10mg/ml, BD 354249)
- Dulbecco's Modified Eagle Medium solution (DMEM, Gibco 11995)
- Reconstruction buffer: Combine 2.2g $NaHCO_3$ (Sigma, S5761) and 4.77g Hepes (Sigma, H3375) into a 100ml medium bottle. Prepare 100ml 0.05N NaOH (Sigma, 38210) by adding 5 ml 1N NaOH to 95 ml distilled H_2O. or you may add 95ml distilled H_2O directly to Hepes and sodium bicarbonate (NaHCO3) powder, mix to dissolve and add a 5 ml 1N NaOH. Then the solution is sterilized by filter (0.2um) and store at -20^{o}C for long term use.

- 5*DMEM: Open a 1 liter package of DMEM powder (Gibco 12800), pour the content into a 200 ml medium bottle, add about 180 ml distilled H_2O (put in graduated cylinder, use this water to rinse the porch), stir for minimum 30 minutes. This solution might never become clear. Then the solution is sterilized by filter (0.2um), the solution will turn clear, adjust the volume to bring a 200 ml with sterile distilled H_2O. Store at -20^oC for long term use.

Step 1: Prepare 5mg/ml fibrin solution

Fibrinogen are dissolved in PBS as 5mg/ml, filtered by 0.22 μm filter at room temperature. Fibrinogen solution is mixed with $Cacl_2$, ACA, and FBS solution at a volume ratio of 1:0.02:0.01:0.01. Leave fibrin stock at room temperature until ready to use.

Step 2: Prepare cell suspensions

Use warm PBS, culture media and serum (FBS) to trypsin cells in flasks, then spin in tube as required density at 1000xg for 4 minutes, remove the medium, leave at room temperature for use.

Step 3: Preparing collagen solution

Reconstruction buffer: 5*DMEM: collagen: DMEM=0.45:0.9:2:1.2. Leave tube containing collagen mixture in ice until ready to use.

Step 4: Preparing thrombin solution

Aliqutoed thrombin (50U/ml) are taken out of refrigerator and dilute to 2.5unit/ml by 1%BSA in PBS at room temperature.

Step 5: Mixing all the components

At room temperature, mix fibrin, collagen and thrombin at a ratio of 9:1:0.5, then with suspended cell at required density, as quickly as possible no more than 10 seconds, then pour in the well-plate or petri dish. The gel are kept in hood untouched for 30 minutes, then transferred into incubator. For petri dishes, a total volume of 2 mL is used. For 96-well plates, 0.1 mL per well is added.

Notes:

The concentration of fibrin, collagen and cell density could be adjusted as required. Above protocol will result in fibrin 4.5mg/ml, collagen 0.45mg/ml and cell 10^6/ml. The ratio of fibrin to thrombin should be always kept in same as 9:0.5 to obtain nice fibrin fibers under microscopy. The pure fibrin gel could be made with similar way, though the ratio of thrombin to fibrin need raise from 0.5 to 1 or 1.5. Otherwise cells will sink in the bottom during period of gel gelation.